Summer 2022

Understanding charge effects on marked ball wear rates – A corrosion study

John Bailey Fletcher

Follow this and additional works at: https://scholarsmine.mst.edu/masters_theses

Department:

Recommended Citation

UNDERSTANDING CHARGE EFFECTS ON MARKED BALL WEAR RATES –

A CORROSION STUDY

by

JOHN BAILEY FLETCHER

A THESIS

Presented to the Graduate Faculty of the

MISSOURI UNIVERSITY OF SCIENCE AND TECHNOLOGY

In Partial Fulfillment of the Requirements for the Degree

MASTER OF SCIENCE

in

METALLURGICAL ENGINEERING

2022

Approved by:

Michael S. Moats, Advisor
Lana Alagha
Laura Bartlett

PUBLICATION THESIS OPTION

This thesis consists of the following two articles, formatted in the style used by the Missouri University of Science and Technology:

Paper I, found on pages 16–40, is intended for submission to *Mining, Metallurgy & Exploration* for publication.

Paper II, found on pages 41–64, is intended for submission to *Mining, Metallurgy & Exploration* for publication.

ABSTRACT

To measure the wear rates of grinding balls within a ball mill, marked ball wear tests (MBWTs) have been used extensively. Using the wear rates from a MBWT, operators select the most cost-effective media for their grinding application. One factor that a MBWT does not account for is the possible interaction between different media materials which could affect their corrosion rates. Galvanic coupling between dissimilar metals can cause significant changes in their corrosion rates. While galvanic interactions between minerals and grinding media have been studied, the interaction between dissimilar media has not. Corrosion rates and potentials of modern high carbon steel (HCS) and high chromium white iron (HCWI) grinding balls were found using an electrochemical testing technique as a function of pH, chloride concentration, and dissolved oxygen content in a simulated mill water (electrolyte). The impact of the chromium content of the grinding media was also evaluated. Through experimental results and application of corrosion theory, galvanic coupling appears to be present between HCS and HCWI in most of the conditions examined. Galvanic coupling was determined to impact corrosion rates significantly. At a 1 to 10 HCWI to HCS surface area ratio (similar to a MBWT where HCWI is added to a HCS charge), HCWI's coupled corrosion rate could decrease by 98% as compared to its uncoupled rate. From these results, operators are cautioned to consider the possibility of galvanic coupling when considering the results of MBWTs.

ACKNOWLEDGMENTS

I would like to start with acknowledging my parents and wife, Marisa, for helping and guiding me towards achieving my goals. Without their love and support, completing my degree would have been exceedingly difficult.

My advisor, Dr. Michael Moats has provided me with endless opportunity. Rescuing me from employment at Taco Bell to presenting fantastic research projects are a few much appreciated moments. I am very thankful for his advice and guidance throughout my research that has certainly prepared me the future.

I want to thank Molycop for funding this project and being a fun group of people to work with. I would also like to thank Dr. Michael Free and Brian Brawley for sharing their corrosion expertise.

I finally would like to thank my research colleagues, Abdul, Florian, Jamie, Joe, Stephen, and Weston for their help in the lab as well as comradery and friendship.

TABLE OF CONTENTS

LIST OF ILLUSTRATIONS

PAPER II

LIST OF TABLES

NOMENCLATURE AND ACRONYMS

Symbol or Acronym	Description
MBWT	Marked Ball Wear Test
HCS	High Carbon Steel
HCWI	High Chromium White Iron
SHE	Standard Hydrogen Electrode
E_{corr}	Corrosion Potential
E_{pit}	Corrosion Pitting Potential
i_{corr}	Corrosion Current
V_{corr}	Corrosion Velocity or Corrosion Rate
I	Current
β_a	Anodic Tafel Slope
β_c	Cathodic Tafel Slope
OCP	Open Circuit Potential
ICP	Inductively Coupled Plasma
$mg\ L^{-1}$	Milligrams per Liter
$g\ L^{-1}$	Grams per Liter
E	Electrochemical Potential
mV	Millivolts
V	Volts

A	Amperes
A cm^{-2}	Amperes per Square Centimeter
μm y^{-1}	Micrometers per Year

1. INTRODUCTION

A primary stage in many mining operations is to crush and grind material for further processing. Grinding alone is a costly operation where small changes can cause large economic consequences. Using ball mills is a frequent grinding practice. Ball mills use steel grinding media to reduce the particle size of rocks by attrition. The consumption of grinding media can be a noticeable cost to many mining operations [1]. Commonly used metals for grinding balls are high carbon steel (HCS) and high chromium white iron (HCWI). The media is subject to abrasion, impact, and corrosion forces [2]. To measure the wear rates of grinding media, marked ball wear tests (MBWTs) are performed and used to select a material to use in the future [3]. Unfortunately, MBWTs do not always produce trustworthy results. It is believed that galvanic coupling interactions may be an underlying cause for these errors.

Corrosion forces are affected by variables such as pH, chloride concentration, and dissolved oxygen content of the mill water [4, 5, 6, 7]. The chromium content of the grinding media is also known to affect the corrosion rate [8, 9, 10]. These factors influencing the corrosion rates of grinding media which in turn alter the consumption rates.

Misrepresenting MBWTs wear rates have led to costly mistakes. Some studies have observed that HCWI being tested in a HCS charge can show HCWI's wear rate to be two to three times less than HCWI's wear rate in a HCWI charge [11, 12]. While this phenomenon has been known, the underlying cause has not thoroughly been investigated.

While the galvanic interaction between minerals and media have been studied [2, 13, 14, 15, 16], the galvanic interactions between dissimilar media has not.

This study examines the potential galvanic interaction between dissimilar grinding ball materials, HCS and HCWI. Commercial samples have been electrochemically tested to find their individual corrosion rates and potentials in various environments. The effects of pH, chloride concentration, and dissolved oxygen in a simulated mill water and the chromium content of the media on the corrosion rates were considered. Using experimental values and corrosion theory, the effects of galvanic coupling on corrosion rates have been modeled as a function of HCWI to HCS surface area ratios.

2. LITERATURE REVIEW

An initial step of many mineral processing operations is comminution. Extracted ore if often reduced to a specific size range to facilitate efficient mineral recovery. A common piece of equipment used to reduce the size of ore is a ball mill. Ball mills are large rotating cylinders that grind ore into smaller sizes with spherical (balls) media. Common grinding ball materials are high carbon steel (HCS) and high chrome white iron (HCWI), with the latter being more wear resistant, but more expensive due to the cost of chromium [17]. Grinding balls are subject to abrasion, impact, and corrosion forces [2], which can lead to noticeable consumption costs at many milling operations [1, 18]. The selection of grinding media is often a balance between cost and consumption rate [19].

A common industrial comparison method of grinding media consumption rate is a marked ball wear test (MWBT). A MBWT adds various types of media to a ball mill during operation to observe their wear rates [3]. Test balls are weighed and marked before being added to an operating mill. Initially, balls were marked by drilling 0.25-inch-deep notches and holes in patterns to identify each ball [20]. These holes can affect the wear rate of the balls, so a new way to mark the balls had to be implemented. An identifying tag is inserted into a single hole and held in place with a low melting point metal [21]. The balls are placed in the operating mill for enough time to wear off a layer of metal approximately 0.125 inches thick [20]. This can take anywhere from 350 to 3000 hours depending on the mill characteristics [21]. Once this time is reached, the mill is stopped and a few of the marked balls are recovered. The low melting point material is

melted out of the ball and the tag is recovered. The weight of the ball is compared to its original weight to determine a wear rate.

Deciding which media to use in the future is dependent on the wear rates and the price of the media. The price of the media is generally governed by the composition [19]. In some scenarios, MBWTs can lead to misrepresented wear rates that can lead to costly mistakes. For example, some studies have shown that HCWI being tested in a HCS charge can show wear rates of HCWI to be two to three times less than the wear rate in a HCWI charge [11, 12]. In other words, performing a MBWT with small amounts of HCWI in a mainly HCS charge, would show that the HCWI's wear rate in this experiment is lower than switching to a solely HCWI charge.

2.1. WEAR MECHANISMS

Because grinding balls are subject to abrasion, impact, and corrosion during milling, researchers have developed tests to measure the resistance of grinding ball materials to these individual consumption mechanisms [22]. Abrasion resistance can be measured using pin-on-drum, dry-sand rubber-wheel, jaw crusher gouging, and impeller-in-drum abrasive wear tests [23]. Impact toughness of grinding balls were determined by Blickensderfer and Tylczak using a J-tube drop tester [24]. Corrosion rates can be evaluated using electrochemical methods [13, 18, 25, 26, 27].

While the resistance of grinding media materials to individual wear mechanisms can be measured, the consumption rate is determined by the synergy of the three mechanisms [23, 27]. By setting up an electrochemical cell that can implement a slurry jet onto a HCWI or HCS sample has allowed some studies [28, 29] to discover effects of

both abrasion and corrosion forces on wear rates. These experiments have led to the

conclusion that when combined, corrosion and abrasion can affect the wear rates more

than the total of each individual force. This has resulted in the industrial usage of

MBWTs to determine the actual consumption rates of grinding balls in a specific

operation because prediction from a laboratory test has proven difficult.

The use of a MBWT, however, creates another difficulty. The potential impact of

galvanic coupling between different media materials has not been thoroughly explored.

Therefore, this study focused on corrosion aspects of wear of modern grinding ball

materials and the assessment of potential galvanic coupling during MBWTs. To assist the

reader in understanding the experimental results and discussion presented in this thesis, a

brief review of corrosion impacts, testing, and terminology is provided.

2.2. CORROSION IMPACTS

Corrosion, or degradation, is an issue that affects every industry that uses

materials. The annual cost of corrosion in the United States in 1982 was estimated to be

between $8 billion and $126 billion [30]. The National Association of Corrosion

Engineers (NACE) estimates that $276 billion were spent in the United States on

corrosion costs in 1998 [31]. Corrosion costs are continuously raising. When neglected,

corrosion forces can not only cause a loss of money, but also become a safety hazard. The

sinking of the Titanic was believed to have been caused by galvanic corrosion [32]. The

ship's hull plates were a different material than the rivets used to hold them in place.

When combined with the corrosivity of seawater, the dissimilar metals caused the plates

to become brittle and prematurely fail when colliding with the iceberg [32]. Every industry is affected by corrosion and the results can be detrimental if neglected.

2.3. CORROSION TESTING

Corrosion is often an electrochemical reaction where a metal returns to a lower energy state, like a metal oxide (rust). For corrosion reactions to occur, the formation of the metal oxide must be favored and the reaction to achieve it must be spontaneous. Oxidation and reduction reactions on the metal's surface are equal and opposite. The oxidation reaction (or anodic reaction) is the metal losing electrons to then form a metal oxide and the reduction reaction (or cathodic reaction) is either oxygen reduction or hydrogen evolution and is gaining electrons. The electrochemical potential is the driving force for these reactions and is always compared to a reference electrode (e.g., standard hydrogen electrode or SHE).

Electrochemical testing equipment can measure the flow of electrons to measure the rates of anodic and cathodic reactions and the corrosion potential (E_{corr}). The linear portion of E vs. log of reaction rates is the Tafel region where the slope is called the Tafel slope. The potential where the reactions are happening at the same rate is the E_{corr}. The Butler-Volmer equation (Equation 1) can use the Tafel slopes and E_{corr} to predict a corrosion current density (i_{corr}) that can be used to calculate a corrosion velocity, or corrosion rate (V_{corr}). In Equation 1, I is the cell current, βa is the anodic or oxidation Tafel slope, βc is the cathodic or reduction Tafel slope, and A is the surface area.

$$I = i_{corr} * A * \left(\exp\left(\frac{2.3(E-E_{corr})}{\beta_a}\right) - \exp\left(-\frac{2.3(E-E_{corr})}{\beta_c}\right)\right) \tag{1}$$

A common corrosion test involves two sequential electrochemical measurements which are used to determine the open circuit potential (OCP), E_{corr}, i_{corr}, and Tafel slopes of a material in a specific solution (e.g., electrolyte). After placing the test sample as the working electrode into an electrochemical cell, the potential is measured with no applied current over time versus a reference electrode. When the working electrode potential has reached a stable reading or after a set duration, the value at this point is considered the OCP for the material in that solution. Immediately following the OCP measurement, potential is scanned from below the OCP to above the OCP at a fixed scan rate while measuring the current. This second measurement is called a potentiodynamic scan. The data from a potentiodynamic scan is typically plotted as electrode potential versus the log of the absolute value of the current density. This plot is called an Evans diagram or a polarization curve, shown schematically in Figure 2.1. The plot illustrates the anodic (oxidation) and cathodic (reduction) behavior of corrosion.
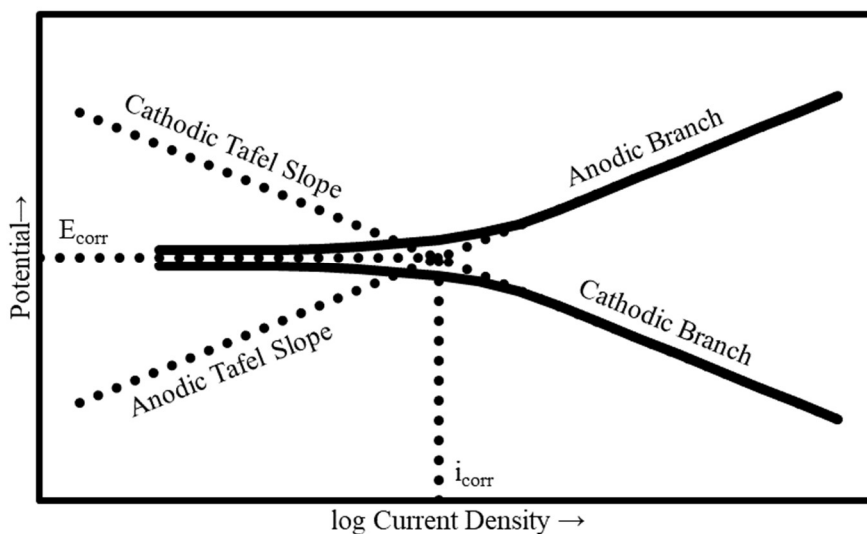
Figure 2.1. Theoretical result of a potentiodynamic scan. The anodic branch represents the oxidation reaction and cathodic branch represents the reduction reaction.

Polarization curves can provide helpful corrosion information. The anodic branch represents the oxidation reaction of corrosion, and the cathodic branch represents the reduction reaction. Where these two reactions occur at the same rate, the E_{corr} of the material exists. At the intersection between the linear Tafel lines and the E_{corr} is the i_{corr} of the material [33]. The i_{corr} of a material can be used to calculate a corrosion velocity (V_{corr}) or corrosion rate using Equation 2, which assumes uniform corrosion is occurring upon the electrode surface. The $1.16 * 10^7$ is a constant for an iron matrix [34].

$$V_{corr} \left(\frac{\mu m}{y} \right) = 1.16 * 10^7 i_{corr} \left(\frac{A}{cm^2} \right) \tag{2}$$

Determining Tafel slopes from real electrochemical data can be challenging and the method varies between studies. The Tafel slope is supposed to represent the active corrosion reactions, but many cases involve passivation and other reactions that can cause difficulties in determining Tafel slopes. A study looking at a hydrogen evolution reaction observes a curve with two separate regions having different Tafel slope values, but of course they both cannot be correct [35]. Another study explores how to calculate the Tafel slopes using polarization resistance techniques rather than potentiodynamic scans [33]. The accuracy in determining the Tafel slope values is crucial when performing a galvanic coupling analysis because small changes can affect the interpretation of results.

For the corrosion of grinding media in mill water, the anodic reaction (oxidation reaction) is the metal dissolution reaction. If a limited current density is reached (current no longer changes with potential), the surface of the material has most likely passivated and active corrosion is no longer being measured [2]. The cathodic reaction (reduction reaction) in grinding media corrosion polarization curves is believed to be oxygen reduction [25]. Stainless steels (similar chromium composition to HCWI) show similar

oxygen reduction behavior in seawater applications [36]. In some scenarios where oxygen is not abundant, the curve could be related to the hydrogen reduction reaction.

2.4. PASSIVATION

During oxidation, certain metals can form protective oxide layers which reduce the corrosion rate of the material. For example, chromium if added to a high enough concentration in iron or steels can help prevent corrosion by the formation of chromium oxide layers during dissolution. These oxides layers are known as a passivation film. Passivation films have helped tremendously in many applications to protect metals from corroding [37]. Some studies have looked at stainless steel (steel containing a minimum of 11 wt% chromium [38]) spray coatings to reduce erosion and corrosion [26, 39]. The formation of a passivation layer on HCWI grinding media occurs during standard laboratory corrosion testing [25]. However, it is believed that the passivated film would be removed due to abrasion in a grinding mill [25]. A previous study introduced inert material in their electrochemical cell and provided ultrasonic agitation to remove this passivation film because it is believed that the film is removed during the grinding operation [25].

2.5. PARAMETERS EFFECTS ON CORROSION

Many variables can affect the corrosion characteristics of grinding media. Different aspects of mill water like pH and chloride concentrations can affect media consumption through changing corrosion rates [4, 13, 25]. Corrosion rates can also be

affected by the amount of dissolved oxygen in the system [5, 6]. The chromium content of grinding media can also impact the corrosion rate [8, 9, 10].

      2.5.1. pH. The pH level of the mill water in a ball mill can change the E_{corr} and i_{corr} values of the grinding media. Carbon steels are understood to have decreasing corrosion rates as pH increases [40]. Stainless steels similarly have decreased corrosion rates with increased pH level environments [41].

      2.5.2. Chloride Content in Solution. Chloride concentration in the mill water solution can change the corrosion aspects of grinding media. Increasing chloride concentration leads to more pitting, or localized penetration into steel surfaces [42, 43, 44]. Using potentiodynamic scans, a corrosion pitting potential (E_{pit}) can be found by sweeping the potential past the Tafel region [45]. Increasing the chloride concentration lowers the E_{pit} value because the chloride ions break through the passivation layer that has formed on the surface of the metal [46, 47]. Another factor to consider is that pitting in 304 stainless steels [46] and carbon steels [47] generally begin at MnS inclusion sites, and the fewer inclusions, the higher the E_{pit} value (lower pitting corrosion rates) [46, 48].

      2.5.3. Dissolved Oxygen in Solution. The availability of oxygen in the system can change the corrosion characteristics of grinding media. A USBM study has claimed that the cathodic reaction in a grinding media polarization curve with a specific simulated mill water solution is oxygen reduction rather than hydrogen evolution [25]. In other words, changing the amount of oxygen available in a ball mill could change the corrosion rates of grinding media. For mild steels, the corrosion pitting rates increase with the amount of oxygen introduced into the system [6]. Hypersteels' (1.2-1.6 C wt%) corrosion rates also increase with the increase of dissolved oxygen [14]. Stainless steels show

accelerated corrosion rates when the oxygen levels increase and can increase corrosion cracking susceptibility [6].

2.5.4. Chromium Content. The amount of chromium in HCWI and stainless steel materials vary from 10.5 to 30 wt%. The corrosion properties change with chromium composition. Stainless steel requires a minimum of 10.5 Cr wt% to ensure the passivation layer forms on the surface [49]. One study compares the chromium to carbon ratio (Cr/C) against i_{corr} values [8]. When the Cr/C ratio is around 15, the i_{corr} values drop two orders of magnitude [8]. The formation of chromium carbides can deplete the iron matrix of chromium that can cause intergranular corrosion [50]. In other words, the overall chromium content of the material can be higher than 10.5%, but chromium carbide formation can deplete iron grains of chromium and cause these depleted areas to corrode. Another study observes that the E_{corr} values decrease with increasing chromium composition [9].

2.6. GALVANIC COUPLING

Galvanic coupling occurs when two dissimilar metals are in electrical contact with each other in an electrolyte solution. If two materials have different electrochemical potentials, then one can act as an anode while the other as a cathode. This effect can cause materials to corrode at different rates when coupled compared to each material individually and has been studied in many different industries. Some studies looked at using galvanic coupling sensors to measure the corrosion of rebar in reinforced concrete [34, 51]. A common way to use galvanic coupling advantageously is to implement a metal as a sacrificial anode. A sacrificial anode, when in a galvanic couple, corrodes to

slow the corrosion rate of the cathode (often the more expensive material). Sacrificial anodes are used to protect ship hulls in the ocean [52, 53] as well as water and natural gas piping in the soil [54, 55].

In wet grinding, many galvanic couples can exist inside of a ball mill. The mill water would act as the electrolyte. Several dissimilar materials exist. The galvanic coupling between grinding media and sulfide minerals has been heavily studied [2, 13, 14, 15, 16] and the potential impact on flotation recovery has been considered [14, 15, 16, 56].

Changing minor aspects of grinding circuits can have effects on downstream processing, such as flotation. Switching grinding media in ball mills has been reported to improve flotation recovery [56]. Another study uses combination potentials between grinding media and sphalerite to show that when the media and ore are galvanically coupled, flotation recovery of the sulfide is negatively affected [14]. A similar study showed that increased galvanic interaction between bornite and grinding media decreased flotation recovery [16].

 Rather than performing potentiodynamic scans, one way to find the coupled corrosion current is to short circuit electrodes and measure the current between them. One study placed either a HCWI (20 Cr wt%) sample or a HCS sample with sulfide mineral samples in electrical contact. The coupling currents indicated that galvanic coupling between the mineral and grinding media could occur. Another conclusion was that the potential of the HCWI was higher than the HCS [13].

Other studies examined the galvanic interactions between minerals and grinding media using potentiodynamic scans to observe coupled corrosion potentials [2, 14, 15,

16]. Different sulfide minerals were compared to a carbon steel sample and two HCWI samples (22 and 29 Cr wt%). The studies showed that chalcopyrite increases all media corrosion rates, galena decreases all media corrosion rates, and sphalerite increases the corrosion rate of the carbon steel and 22 Cr wt% HCWI sample but decreases corrosion rate of 29 Cr wt% HCWI sample by galvanic coupling [2]. Other HCWI samples (15, 21, and 30 Cr wt%) displayed less galvanic interaction with arsenopyrite than a mild steel sample [15]. A sphalerite slurry was shown to increase the corrosive wear of hypersteel (1.2-1.6 C wt%) in a galvanic couple as well [45].

The galvanic coupling interaction between media and minerals can be affected by the dissolved oxygen in the system. When coupling various medias with arsenopyrite, sphalerite, and bornite, increasing the amount of dissolved oxygen increases the galvanic interactions between media and sulfide minerals [14, 15, 16].

Corrosion potentials for various grinding media have also been measured. A HCS sample and four HCWI samples (4.5, 8.5, 12.5, and 14.5 Cr wt%) were electrochemically tested. The differences found in the potentials can lead to the prediction that when coupled, corrosion pitting intensifies in a HCS sample and reduced corrosion pitting is found in a HCWI sample compared to their individual corrosion rates [11].

2.7. OBJECTIVES

Thus, the possible galvanic interaction between dissimilar grinding media materials with a wide range of chromium contents have not been thoroughly studied. One goal of this study is to observe corrosion rates modern grinding media materials in solutions with different pH, chloride concentration, and dissolved oxygen levels. The

rates will also be obtained for grinding media with differing chromium compositions. The second goal of this study is to show the effects of galvanic coupling on corrosion rates of HCS and HCWI when they are in electrical contact.

Paper I discusses the effects of pH and chloride concentrations on the corrosion rates of one HCS and one HCWI composition. pH levels included 3, 5, 7, 9, and 11 while chloride concentrations were 1, 2, and 4 g L^{-1}. Paper I uses Tafel slopes, E_{corr}, and i_{corr} values from the corrosion rate experiments as well as corrosion theory to predict the corrosion rates of HCS and HCWI when they are in a galvanic couple. The paper contains a thorough explanation of how galvanic coupled corrosion rates are obtained from potentiodynamic scans. The impact of different surface area ratios of HCWI:HCS on galvanic coupled corrosion rates are compared to individual corrosion rates of the materials.

Paper II reports the corrosion rates for several samples of HCS and HCWI with various chromium contents and simulated mill water with two levels of dissolved oxygen concentrations. For the HCS samples, the addition of 2 Cr wt% is analyzed and the HCWI samples vary from 14 to 28 Cr wt%. Corrosion rates are obtained with the simulated mill water being air or nitrogen sparged at a pH of 7 or 11. The results are used to examine the impact of galvanic coupling between the HCWI samples and one HCS composition.

2.8. EXPERIMENTAL LIMITATIONS

The following studies aim to find corrosion characteristics of grinding media in a simulated mill water. The media corrosion rates in industry can be affected by the

composition of the mill water, so each individual mining operation could have different results based on the composition of their mill water. Another limitation of this study is the effect of temperature. All experimenters in this study were performed at the ambient temperature of the laboratory (ca. 22 °C) but in reality, the temperature in ball mills vary. The corrosion rates of steels and other materials are affected by the temperature of their environment [57].

The experimental setup in this study required the surface of the sample to be polished before corrosion testing began. The microstructure of the sample could change throughout the sample and effect the corrosion characteristics. Certain types of balls can have varying microstructures from surface to center of the ball [21]. The inclusions present in the microstructures were also not characterized in this study. Because some inclusions are known to cause corrosion [46, 48], characterizing them could also help determine underlying corrosion driving forces.

PAPER

I. UNDERSTANDING CHARGE EFFECTS ON MARKED BALL WEAR RATES – A CORROSION STUDY: PART 1. THE IMPACTS OF pH AND CHLORIDE CONCENTRATION

John Bailey Fletcher and Michael S. Moats

Materials Research Center
Department of Materials Science and Engineering
Missouri University of Science and Technology
Rolla, MO, USA 65409

ABSTRACT

Marked ball wear tests have been used extensively to evaluate the consumption of different grinding media types during industrial ball milling. The possible galvanic interaction of media materials during marked ball wear tests has not been adequately explored. Corrosion rates and potentials of modern high carbon steel and high chromium white iron grinding media materials were measured using electrochemical testing as a function of pH and chloride content in a simulated mill water. The results replicate previous research with the high chromium white iron sample being more noble (higher corrosion potential) and corrosion resistant (small corrosion current) than high carbon steel. Using the experimental data and corrosion theory, the effects of galvanic coupling on corrosion rates were calculated to examine what could happen during a marked ball wear test or when a mixed media charge is present. This analysis indicates that high carbon steel can cathodically protect high chromium white iron leading to significant

decreases in the corrosion rate (up to 99%) of this material during marked ball wear tests. The magnitude of the protection is a function of the pH of the mill water.

1. INTRODUCTION

In many mining operations, crushing and grinding are necessary comminution stages prior to mineral beneficiation. Specifically, grinding is a costly unit operation where small changes can result in large economic consequences. Ball milling is a common grinding practice, which uses grinding balls to reduce the size of ore to aid in further processing. Grinding balls or media are subject to impact, abrasion, and corrosion forces that lead to their inevitable demise [1]. Grinding media consumption is a noticeable cost to many mining operations [2].

High carbon steel (HCS) and high chromium white iron (HCWI) are commonly used materials for grinding balls. Selection of grinding media material is often a balancing of the consumption rate and cost [3]. Consumption rate depends upon the operating conditions of the mill and the abrasiveness of the ore. Environmental conditions such as pH and chloride concentration can affect media consumption due to corrosion [4,5]. Some operations have also experienced improved flotation recovery by switching media material [6].

Operations conduct plant trails to examine the consumption rates of different media materials using a marked ball wear test (MBWT) [7]. A MBWT is performed by adding marked prospect grinding balls to the mill during operations and then observing

the wear rates after a period of time. Wear rates are then used to determine which media material results in a lower grinding cost for the operation.

There are indications in the literature that wear rates determined by MBWT may be influenced by the predominant charge material. Industrial data indicate that when HCWI is tested in HCS charges, the wear rate of HCWI could be two to threefold less than wear rates measured in HCWI charges [8,9]. While this potential influence has been known, the underlying phenomenon has not been investigated.

In this study, the interaction between grinding media material was investigated by examining the possibility of galvanic coupling of HCS and HCWI. To conduct this investigation, the corrosion potential and currents of commercial HCS and HCWI materials were measured in a laboratory setting as a function of pH and chloride concentration. The electrochemical data were then used to predict the possibility of galvanic coupling and the resulting impact on corrosion rates.

2. METHODS

Specimens of high carbon steel (HCS) and high chromium white iron (HCWI) were obtained from four commercial balls by an industrial supplier. The compositions of the specimens are provided in Table 1. Electrodes were fabricated by water jetting a 1 cm x 1 cm section from the commercial specimens. The section was attached to a copper wire with conductive silver paint and encased in epoxy. The face of the section was exposed by grinding and polishing. Images were taken of each electrode surface and analyzed using ImageJ to obtain a precise surface area measurement [10].

Electrochemical testing was performed in a three-electrode cell, Figure 1. The working electrode was the fabricated grinding media sample. The counter electrode was an iridium-tantalum oxide coated titanium mesh because of its availability, stability, and ability to pass oxidation and reduction currents in aqueous solution. The reference electrode was a saturated mercury/mercurous sulfate electrode (0.64 V vs. SHE). Potentials were converted and reported relative to the standard hydrogen electrode (SHE).

Table 1. Chemical composition of grinding media samples. Compositions were measured by inductively coupled plasma (ICP) using ASTM E2594-20 modified [19] and ASTM E1019-18 [20] methods.

Weight %	HCS A	HCS B	HCWI A	HCWI B
Chromium	0.32	0.32	23.21	23.37
Carbon	1.07	1.01	2.57	<0.01
Manganese	0.83	0.83	0.32	0.34
Silicon	0.15	0.15	1.09	1.14

250 mL of synthetic simulated mill water with a composition described in Table 2 was used as the electrolyte. This solution composition was selected to allow for comparison with previously grinding media corrosion studies conducted by the U.S Bureau of Mines (USBM) [11]. Air was sparged into the cell and produced a dissolved oxygen level of 6.6 mg L^{-1} in the mill water prior to testing.

The USBM study indicated the need to remove corrosion products to avoid passivation which would likely occur during wet grinding [11]. Therefore, 10 g L^{-1} of 48-mesh alumina polishing powder was added to the cell and suspended using external

stirring. The effectiveness of this method to remove the passivation layer from the

grinding media will be demonstrated in the results section.

Figure 1. The three-electrode corrosion cell setup. The reference electrode is in the left neck, the working electrode is in the middle neck, and the counter electrode and sparging tube are in the right neck.

Table 2. Dissolved salt concentrations of the simulated mill water.

Solute	Concentration ($g\ L^{-1}$)
NaCl	2.51
KCl	0.15
$MgCl_2*6H_2O$	1.09
$CaSO_4*1/2H_2O$	1.01

Electrochemical testing was performed using a Gamry Reference 3000

potentiostat to control and/or measure current or potential. Electrochemical testing

consisted of a two-step measurement process. The initial measurement was to determine

the open circuit potential (OCP). OCP was obtained by measuring the potential at open

circuit conditions over time. The OCP measurement occurred for 15 minutes or less if

potential changed less than 0.01 mV per second. The OCP value was the last recorded

potential measurement. The OCP was used in the second step of the electrochemical test,

a potentiodynamic scan. A potentiodynamic scan was performed by sweeping the

potential from -200 mV vs. OCP to +150 mV vs. OCP at a rate of 0.5 mV sec^{-1} while

measuring the resulting current.

The potentiodynamic data were processed to obtain the current density using the

measured surface area of the electrode used in the test. The electrode potential was

plotted versus the absolute value of the current density to obtain a polarization curve

(e.g., an Evans or corrosion diagram). The corrosion potential (E_{corr}), corrosion current

density (i_{corr}), and Tafel slopes were obtained from the polarization curves. The corrosion

velocity, or corrosion rate (V_{corr}) was calculated using Equation 1. The value $1.16*10^7$ is

a constant used for an iron matrix [12].

$$I = i_{corr} * A * (\exp\left(\frac{2.3(E - E_{corr})}{\beta_a}\right) - \exp\left(-\frac{2.3(E - E_{corr})}{\beta_c}\right)) \tag{1}$$

Each sample was tested in various electrolyte conditions which are summarized in

Table 3. 0.1 M H_2SO_4 or 0.1 M NaOH solutions were used to adjust the starting pH to the

target experimental value. Total chloride concentration was achieved by the addition of

NaCl to the electrolyte.

Table 2. Electrolyte conditions. These were used to examine the impact of pH and chloride concentration on grinding media corrosion.

Material	pH	Total Cl$^-$ concentration (g L^{-1})
HCS	3, 5, 7, 9, 11	2
HCWI	3, 5, 7, 9, 11	2
HCS	7, 9, 11	1, 2, 4
HCWI	7, 9, 11	1, 2, 4

3. RESULTS

Electrochemical testing can elucidate corrosion current (i_{corr}) and corrosion potential (E_{corr}) for a metallic material for specific environments. Figure 2 is a schematic example of a polarization curve obtained from a potentiodynamic scan. The anodic branch shows the reaction rate of the oxidation reaction or metal corrosion when the potential is more positive than the corrosion potential. The cathodic branch shows the reaction rate of the reduction reaction, commonly reduction of dissolved oxygen or hydrogen cations when the potential is more negative than the corrosion potential. When the two rates (for example, metal corrosion and dissolved oxygen reduction) are equal, this occurs at the material's E_{corr} value. The polarization curve at least 50 mV away from E_{corr} (e.g., high field approximation of the Butler Volmer equation) produces a linear region on an Evans diagram. The slope of the linear region is called the Tafel slope [13]. When the linear portion of the anodic and cathodic branches are extended to the E_{corr} value, the lines intersect at a point. The current density at that point is the material's i_{corr},

which is the corrosion rate of the metal in the environment tested assuming no

passivation occurs with time and there are no mass transport limitations due to reagent

consumption.
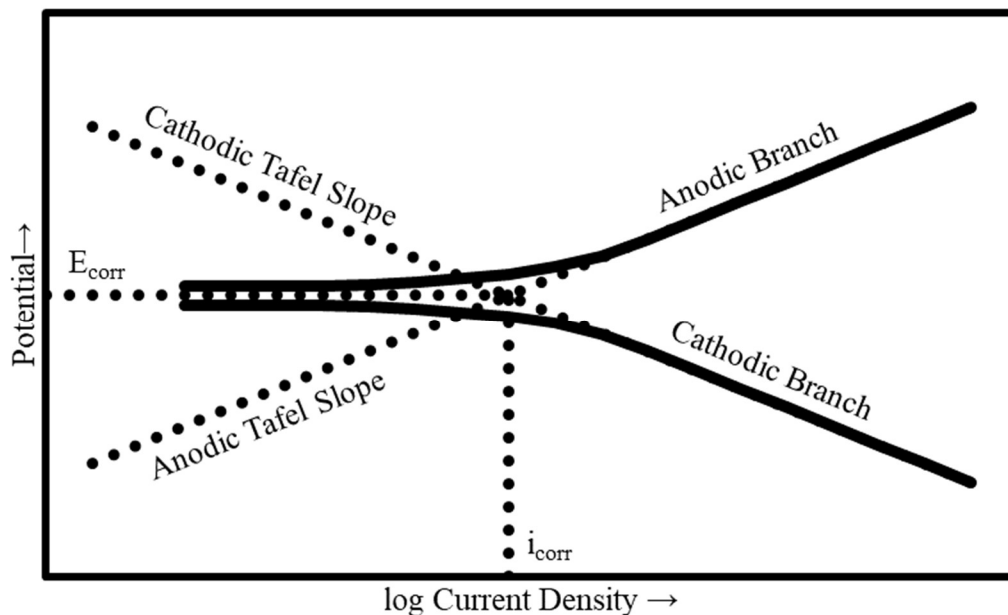
Figure 2. A schematic ideal potentiodynamic data set. Shown are how the i_{corr}, E_{corr}, and Tafel slopes are determined.

Initial testing proved that like the previous USBM grinding media study [11], the

removal of corrosion products and/or passivating films is needed to generate reproducible

and representative results. An initial potentiodynamic scan without stirred alumina

powder in the testing cell is shown in Figure 3. The results show a vertical anodic branch

at potentials more positive than -0.4 V vs. SHE. This indicates the metal surface became

passive due to the formations of a corrosion product during the test. Since grinding media

are known to have shiny surfaces when quickly examined after a mill is stopped, the

formation of a passive film during grinding is not believed to occur but is removed by abrasion. Stirring 10 g L 1 48# alumina powder during the electrochemical test was able to remove the passivation layer long enough to produce a region of active corrosion to determine the Tafel slope as the results displayed in Figure 4 demonstrate. Thus, all corrosion experiments were conducted in conjunction with the stirring of alumina in the solution.
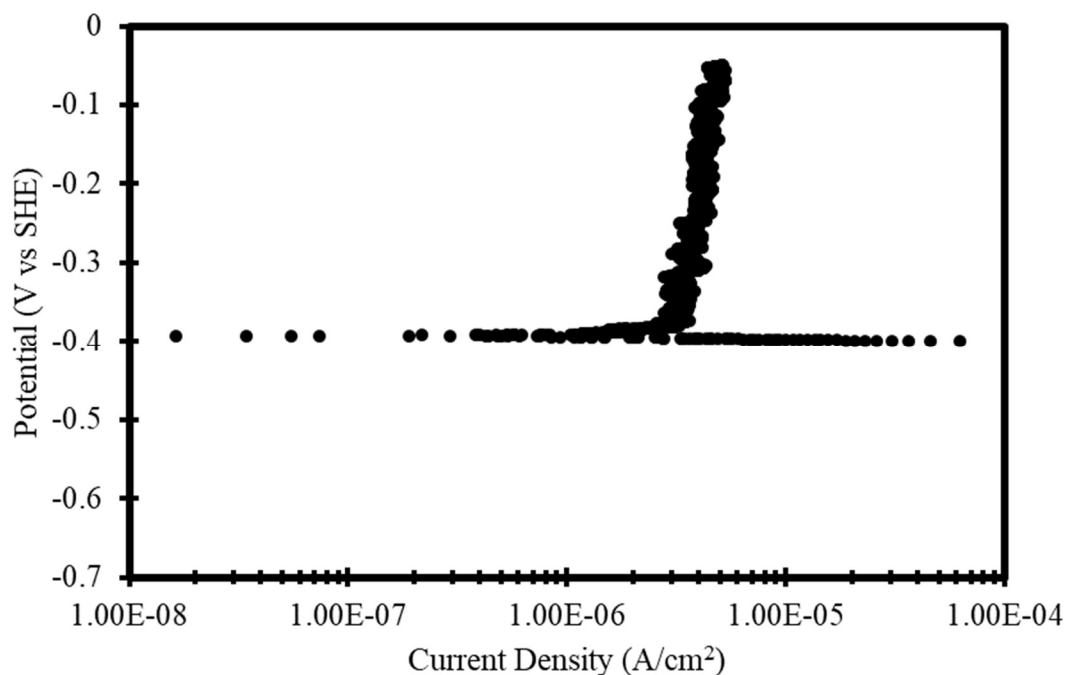
Figure 3. A potentiodynamic scan of HCS in aerated simulated mill water at a pH of 7 without the addition of stirred alumina powder. Scan rate is 0.5 mV s^{-1}.

Data for HCWI and HCS in a solution with a pH of 7 and chloride concentration of 2 g L^{-1} are shown in Figure 5. The E$_{corr}$ values exist were both reaction branches have the same potential value and were determined by the Gamry Tafel fit tool. The Tafel lines for each data set and branch are overlayed within the plot. Tafel lines were determined by

placing two points in the Gamry E log i program to calculate a slope. The initial point

placed was at least 50 mV above or below the E_{corr} value and the second point was placed

where the slope became non-linear. Where one Tafel slope intersected the E_{corr} value is

the i_{corr} value. This method led to two slightly different i_{corr} values and the average values

for each test are displayed with their respective data set. For Figure 5, HCWI Tafel lines

are the dashed lines and the HCS Tafel lines are the solid lines.
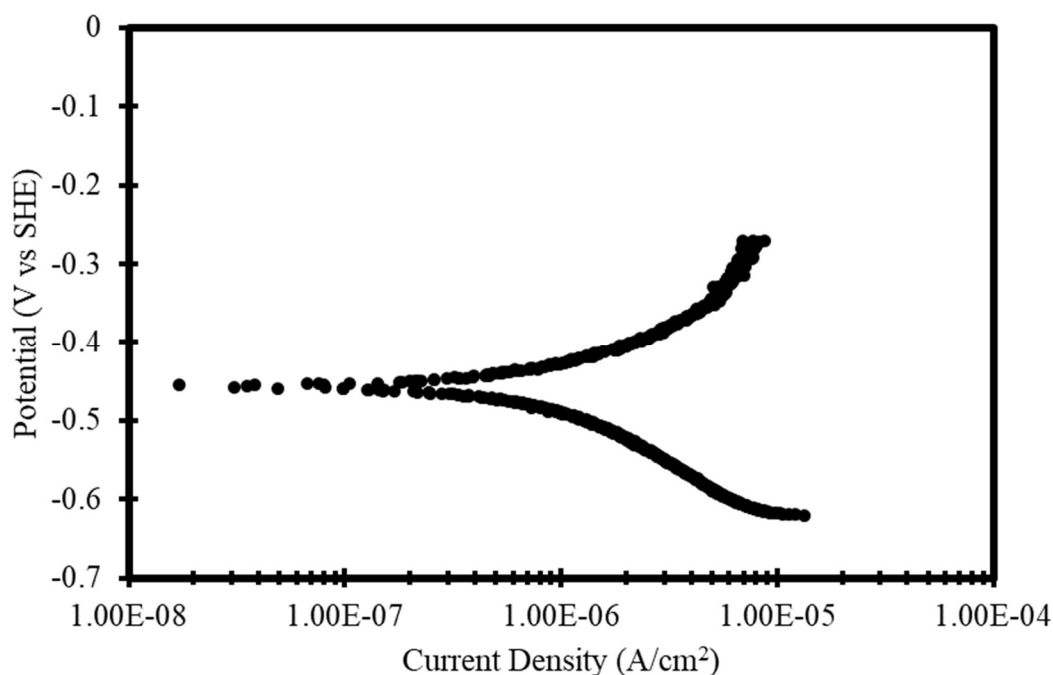
Figure 4. Potentiodynamic scan of HCS in aerated simulated mill water at a pH of 7 with the addition of stirred alumina powder. Scan rate is 0.5 mV s^{-1}.

The effect of pH on E_{corr} values for HCS and HCWI in simulated mill water is

illustrated in Figure 6. As expected, HCS has a lower E_{corr} value than HCWI at all pH

levels from 3 to 11. The HCWI E_{corr} value is not significantly affected by pH with values

ranging between 0 and -0.1 V vs. SHE. The HCS E_{corr} values show consistent values

from pH of 7 to 11 at -0.23 V vs. SHE, which is the operating pH of many grinding

applications for mineral beneficiation. As the pH decreases to 3, the E_{corr} value shifts to a

more negative value of ca. -0.35 V vs. SHE and which signifies that it is more likely to

corrode at those conditions.
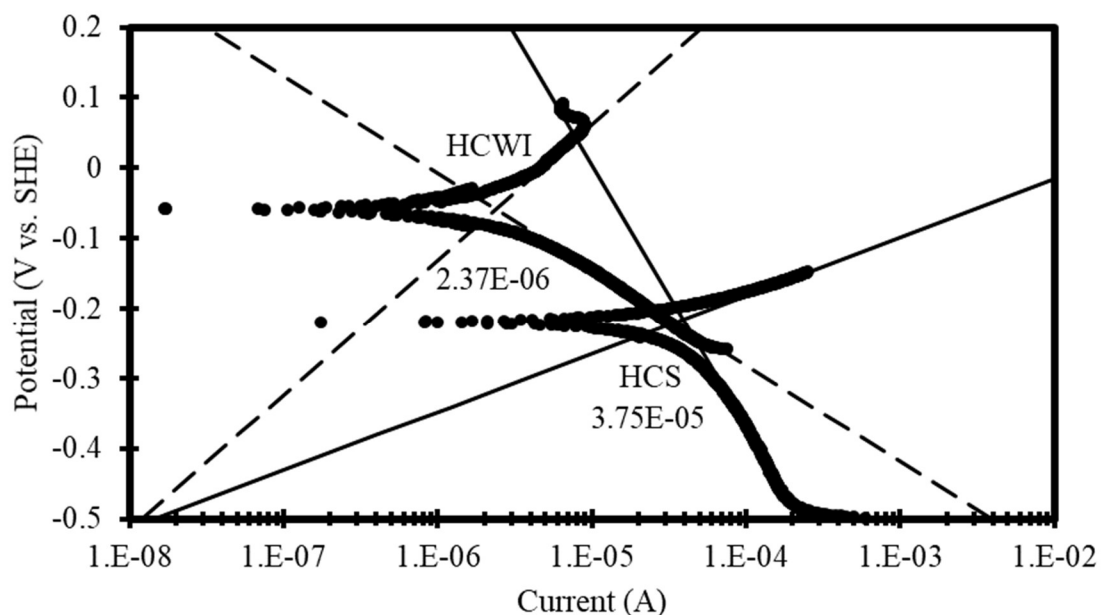
Figure 5. Two sets of corrosion data: HCWI and HCS at a pH of 7. The i_{corr} values of
each individual experiment are displayed with their respective data set.

The corrosion rates or V_{corr} values for HCS and HCWI in simulated mill water as

a function of pH is displayed in Figure 7. HCWI exhibits 1-2 orders of magnitude lower

corrosion rates than HCS at all pH levels. At a pH of 3, both materials show higher

corrosion rates than other pH levels. HCS shows a more consistent V_{corr} between 100 and

1000 micrometers per year than HCWI's V_{corr}, which appears to decrease from 50 to 3

micrometers per year as pH increases from 5 to 11.
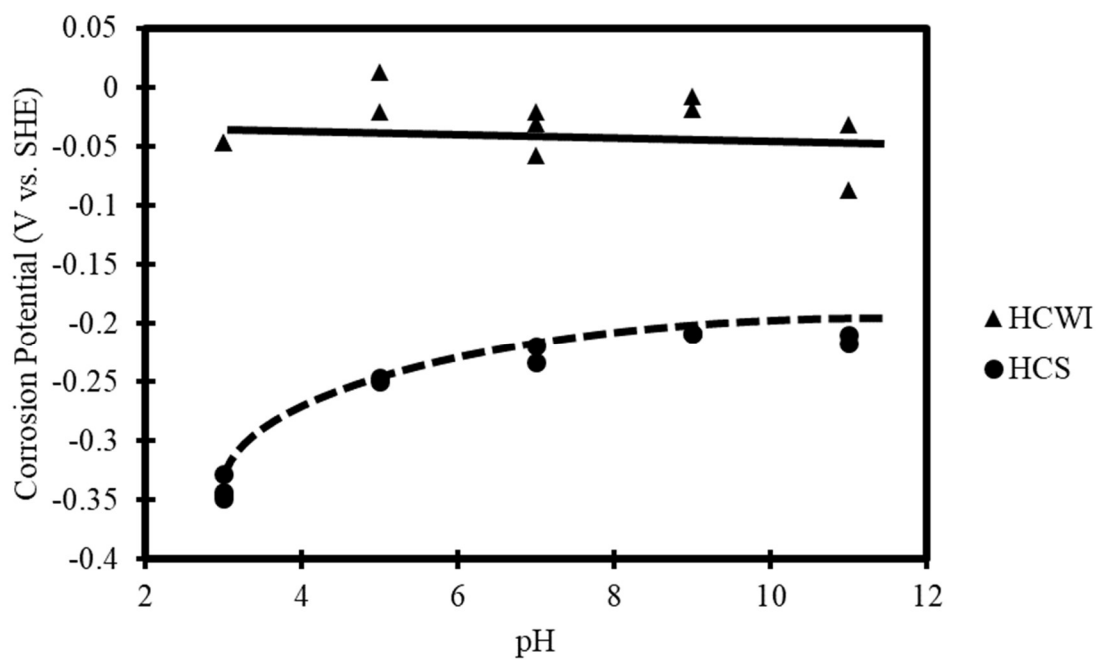
Figure 6. E_{corr} values for HCS and HCWI as a function of pH in aerated simulated mill water.
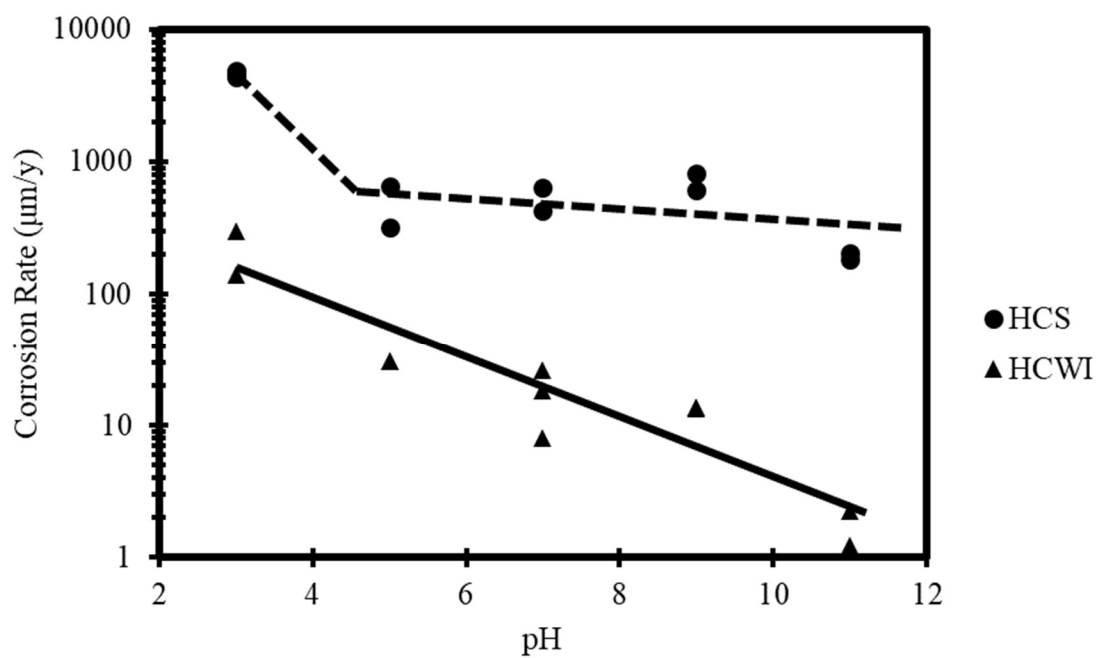
Figure 7. V_{corr} values for HCS and HCWI as a function of pH in simulated mill water.

Figures 8 and 9 depict the E_{corr} and V_{corr} values, respectively, versus chloride concentration in simulated mill water at three pH levels. The corrosion potential for HCS and HCWI, at these specific conditions, do not appear to be significantly affected by the change in chloride concentration. Similarly, chloride concentration is shown to generate little to no effects on the corrosion rates of either material in these specific conditions.
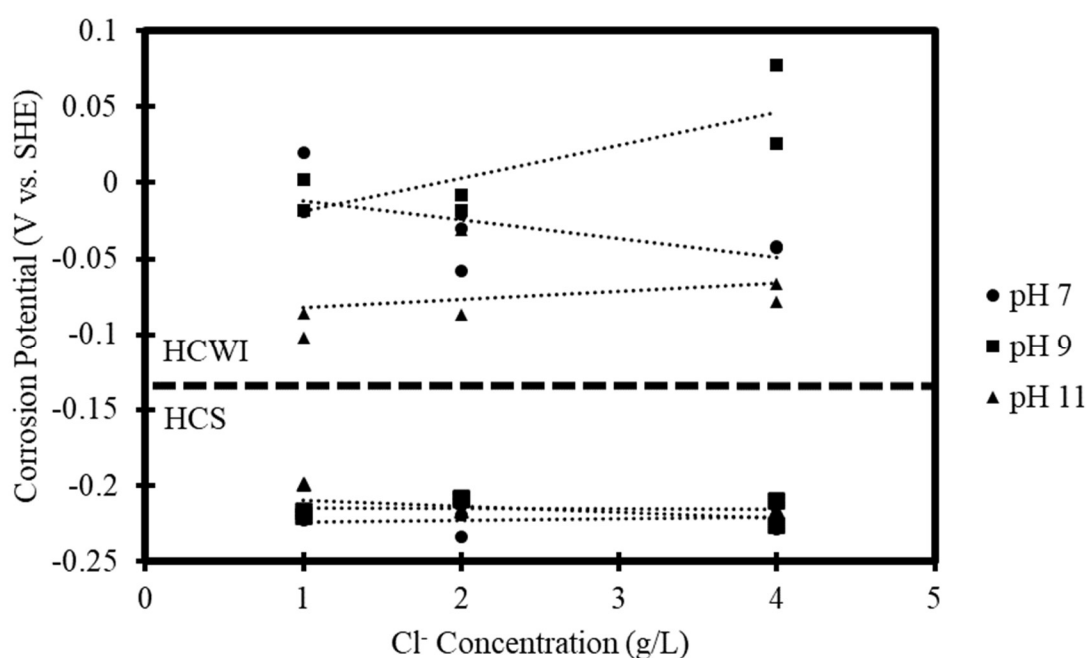
Figure 8. E_{corr} values as a function of chloride concentration for HCS and HCWI at pH levels of 7, 9, and 11 in simulated mill water.

4. DISCUSSION AND ANALYSIS

All data indicate that the HCWI has a higher E_{corr} than the HCS. This is because the HCWI is a more noble material than the HCS, leading to a scenario that could generate a galvanic couple when the two materials are in electrical contact with each

other. Another consistent and expected observation is that the corrosion rates for HCS are

higher than HCWI in all solutions. As pH decreases, both materials show higher

corrosion rates. This is most likely because of the increased availability of H+ that supply

the reduction reactions [3].
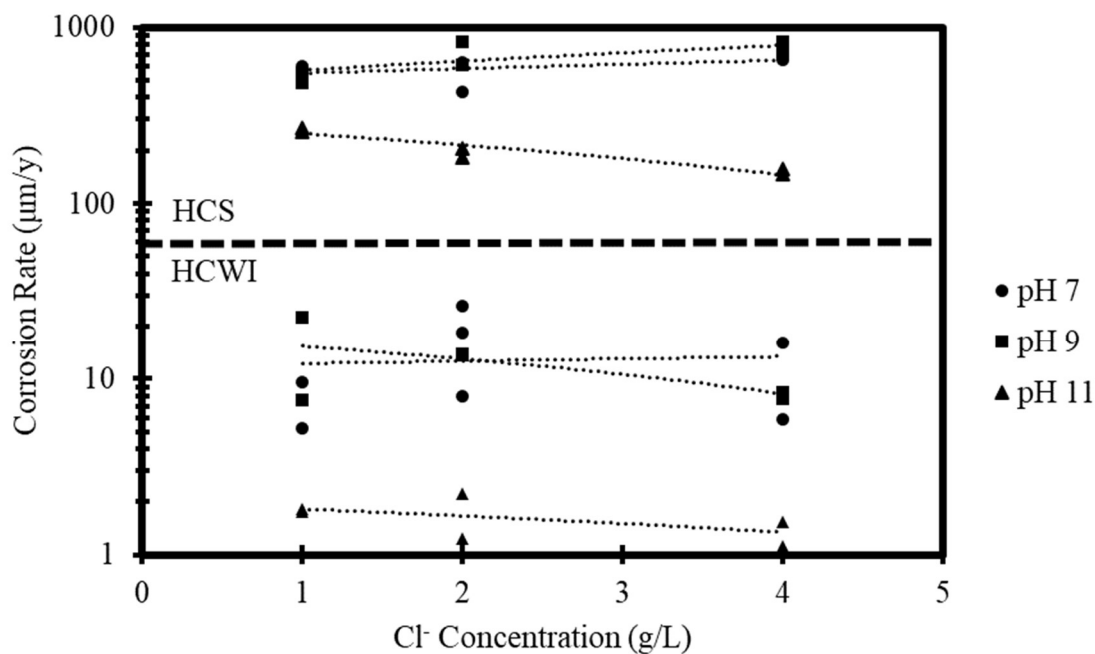
Figure 9. V_{corr} values as a function of chloride concentration for HCS and HCWI at pH
levels of 7, 9, and 11 in simulated mill water.

This testing indicates that chloride concentration did not affect either E_{corr} or V_{corr}.

Increasing chloride concentration is known to cause corrosion pitting, or chloride ion

penetration [14]. Pitting corrosion can be detected by electrochemical testing [15]. The

testing method used in this study avoided passivity and did not scan to positive enough

potentials to observe the behavior seen in other studies. Other studies showing chloride

affecting corrosion rates used higher chloride concentrations, such as 1 and 2 M, and in

deaerated environments [16, 17]. Additional work is needed to examine the impact of pitting on grinding media corrosion behavior.

The electrochemical data from a potentiodynamic scan can be used to examine if metals will exhibit galvanic coupling if they are placed in physical contact in the environment being studied. Galvanic coupling is possible when two dissimilar metals are in electrical contact which allows for electron exchange and in a common electrolyte or solution to allow for ion transport needed for electrochemical reactions.

Every galvanic coupling cell consists of an anode and a cathode. Oxidation occurs at the anode and reduction occurs at the cathode. In a galvanic cell, the anode can be called the sacrificial anode because it is oxidizing, or being sacrificed, rather than the material which serves as cathode. The anode has a lower electrochemical potential (E) than the cathode for this to occur.

The surface potential of HCS was found to be more negative than HCWI in all conditions examined, which confirmed previous research [4, 8, 11]. Thus, when these grinding materials are in electrical contact within a common conductive solution (e.g., balls touching in the charge during wet grinding), the anode would be HCS and the cathode would be HCWI.

Figure 10 shows the implications of galvanic coupling on the i_{corr} values of each material. The dashed arrows represent the i_{corr} of the two materials when they are not in electrical contact. This would represent the corrosion rate of HCWI in a HCWI charge and HCS in a HCS charge. The solid arrows represent the i_{corr} values when HCS and HCWI are galvanically coupled. The coupled point is where the total cathodic rate (sum of cathodic reaction on HCWI and on HCS) and total anodic rate are equal (shown as the

intersection of the Total Cathodic and Total Anodic lines). At this point, both materials have the same E_{corr} value called the coupled E_{corr}. At the coupled E_{corr} value, i_{corr} of each media is determined as the corrosion rate of the anodic curve at that potential. These are shown as solid arrows. Hence, the corrosion rate of HCWI decreases when coupled with HCS and the i_{corr} of HCS increases when coupled with HCWI. In other words, when HCS and HCWI are in electrical contact within a grinding mill, HCWI's corrosion rate decreases and HCS's corrosion rate increases. HCS serves as a sacrificial anode to HCWI, which is cathodically protected.

The galvanic coupling effect using the data presented in Figure 5 is displayed in Figure 11. The analysis assumes the surface area of HCS and HCWI are the same. Tafel lines for each test and the total reactions are displayed to show how the new coupled i_{corr} values are determined. Using the method in Figure 10, the coupled i_{corr} values for HCS and HCWI are 6.02 x 10^{-5} and 4.37 x 10^{-7} A cm^{-2}, respectively. The coupled corrosion current density of HCWI is 1.93 x 10^{-6} A cm^{-2} lower than the corrosion current density of HCWI alone. On the contrary, the coupled corrosion current density of HCS is 2.27 x 10^{-5} A cm^{-2} larger than the corrosion current density of HCS alone. In other words, the corrosion rate of HCWI decreases and the corrosion rate of HCS increases when coupled.

Figure 12 modifies the data from Figure 5 to examine a surface area ratio of 100:1 for HCWI to HCS. The curves are the same as Figure 11, except the HCWI reaction has been shifted 100 x in the positive current direction. Changing the surface area ratio changed the total reaction rate curves to affect the coupled i_{corr} values for both materials. HCWI's coupled corrosion rate still decreased when compared to its individual corrosion rate by 1.22 x 10^{-6} A cm^{-2}. HCS's coupled corrosion rate is still higher by 5.24x10^{-4} A

cm^{-2}. Figures 11 and 12 show that at both surface area ratios, HCWI's corrosion rate

decreases and HCS's corrosion rate increases during electrical contact.
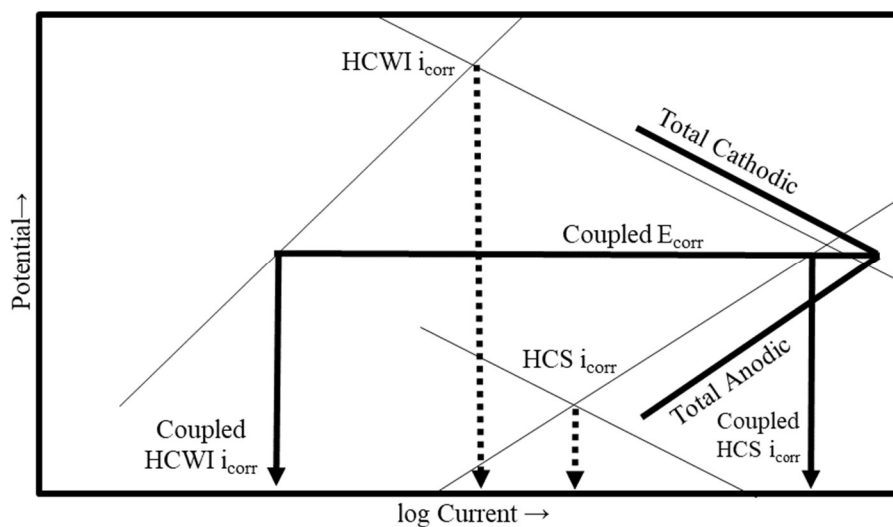
Figure 10. A schematic example of two potentiodynamic data sets (HCS and HCWI in the same environment with a surface area ratio of 1:1 and how galvanic coupling affects their i_{corr} values.
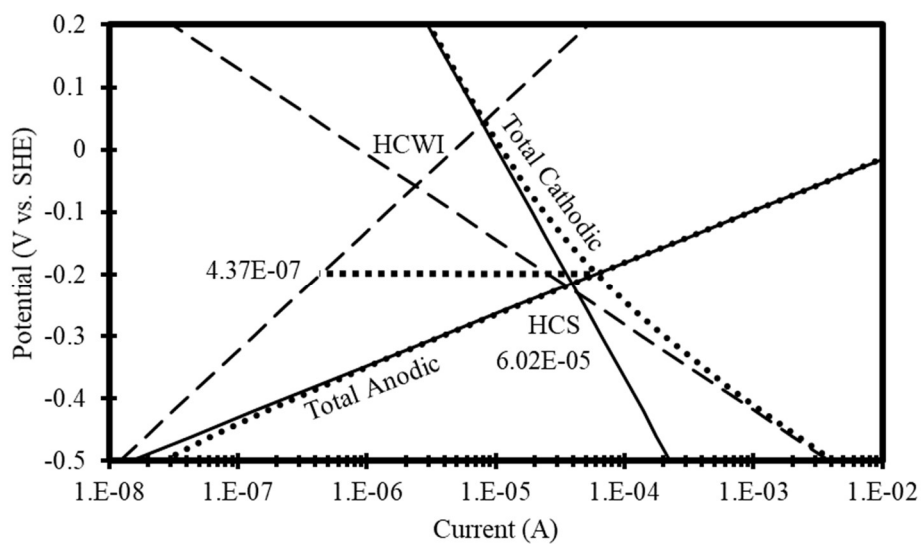
Figure 11. Galvanic coupling analysis of electrochemical data presented in Figure 5 with the coupled i_{corr} values displayed assuming a surface area ratio of 1:1 for HCWI:HCS.
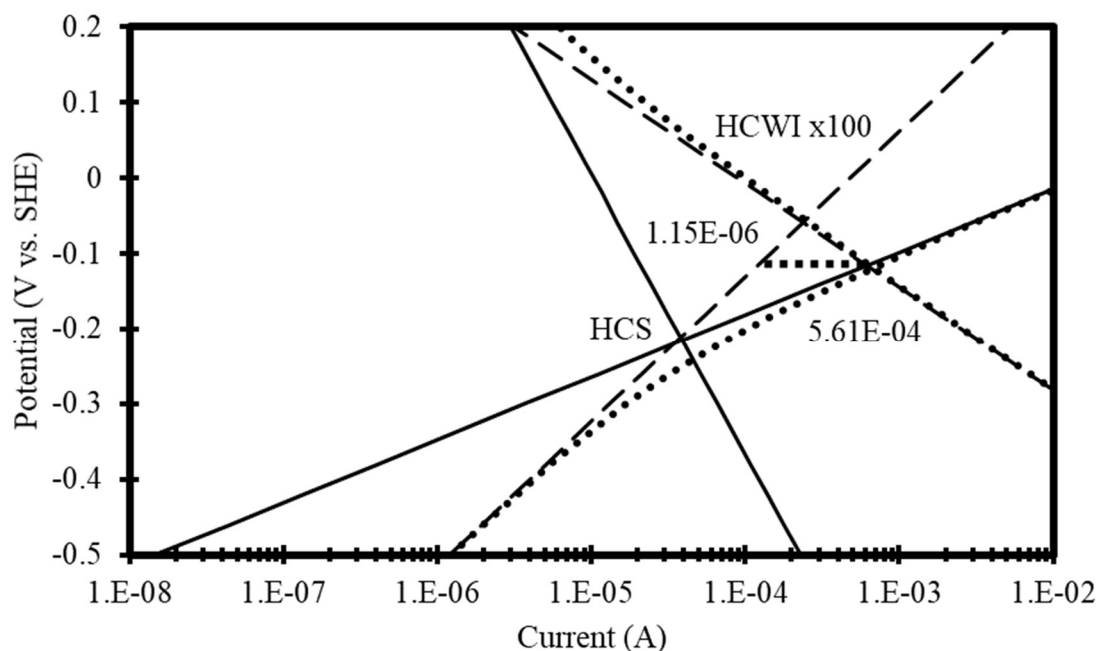
Figure 12. Galvanic coupling analysis of electrochemical data presented in Figure 5 with the coupled i_{corr} values displayed assuming a surface area ratio of 100:1 for HCWI:HCS.

Changing the surface area ratio between HCWI and HCS results in different corrosion rates for each material. Figure 13 displays the corrosion rate results from Figures 11 and 12 along with other surface area ratios. The individual V_{corr} values for each material are shown as the dashed lines. The difference between the dashed line and the data points is the corrosion rate change when individual V_{corr} values are compared to the coupled V_{corr} values. At a surface area ratio of 1:100 and 1:10 HCWI to HCS (displayed as 0.01 and 0.1, respectively), the coupled V_{corr} of HCS is the same as its individual V_{corr}. This indicates that HCS corrosion rate does not likely change during a MBWT when HCWI is introduced to a HCS charge. On the other end at 100:1 HCWI to HCS, the coupled V_{corr} for HCWI is 14 μm y^{-1} lower than the individual V_{corr} value, showing that a minimal amount of HCS could lower HCWI's corrosion rate.
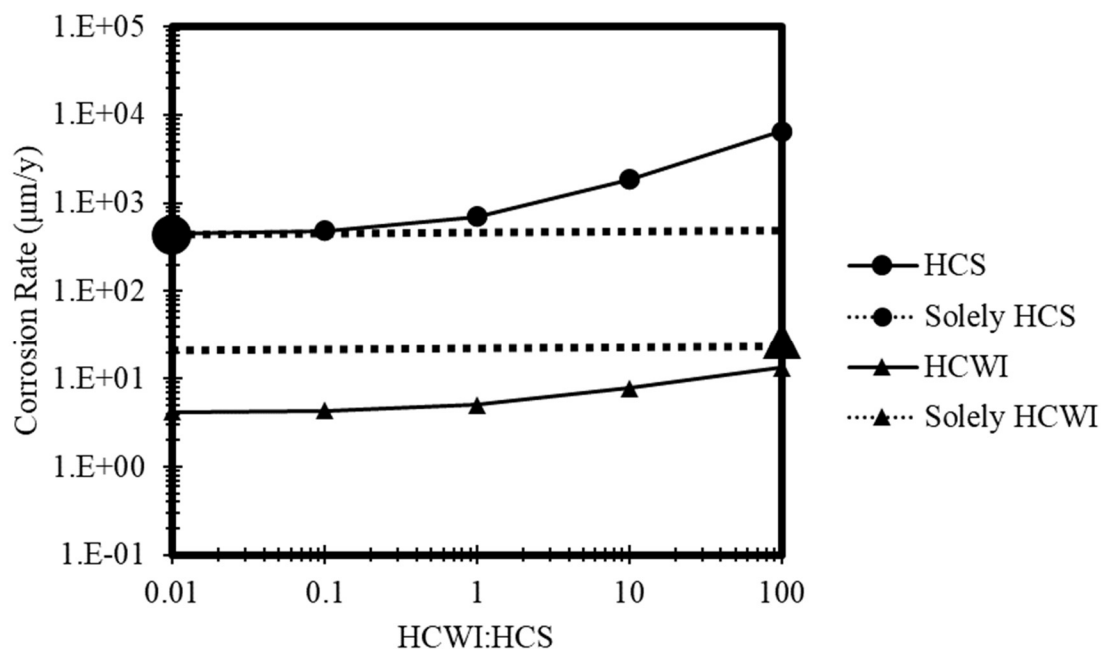
Figure 13. The effect of surface area ratios on couple corrosion rates in pH 7 aerated simulated mill water. The dashed lines represent the V_{corr} values for each material individually and the solid data sets represent coupled V_{corr} values.

Figures 14-17 show the effects of surface area ratios of HCWI:HCS on corrosion rates in different pH environments. As pH rises, the individual and coupled corrosion rates decrease. pH levels of 5, 7, and 9 show similar results while a pH of 11 produced lower individual and coupled V_{corr} values for both materials. A pH of 11 reveals the largest differences between the individual and coupled V_{corr} values for the HCWI. At a 1 HCWI to 1 HCS ratio, the coupled corrosion rate of HCWI is 93 x smaller than its individual corrosion rate while the coupled HCS corrosion rate only slightly changes. Having a 1 HCWI to 1 HCS surface area ratio in a pH of 11 can decrease HCWI's corrosion rate substantially while sacrificing a negligible amount of HCS.
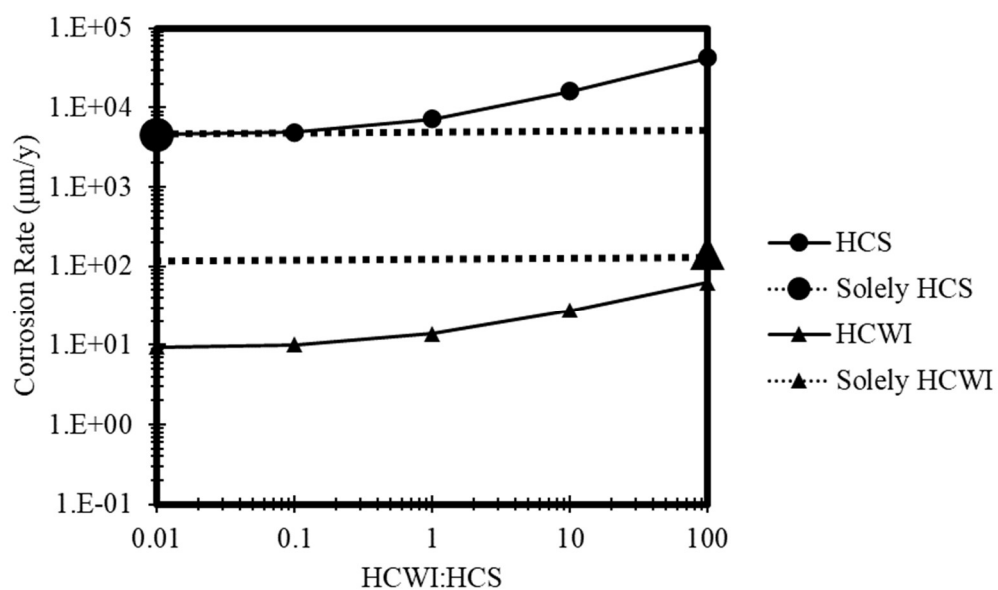
Figure 14. The effect of surface area ratios on couple corrosion rates in pH 3 aerated simulated mill water. The dashed lines represent the V_{corr} values for each material individually and the solid data sets represent coupled V_{corr} values.
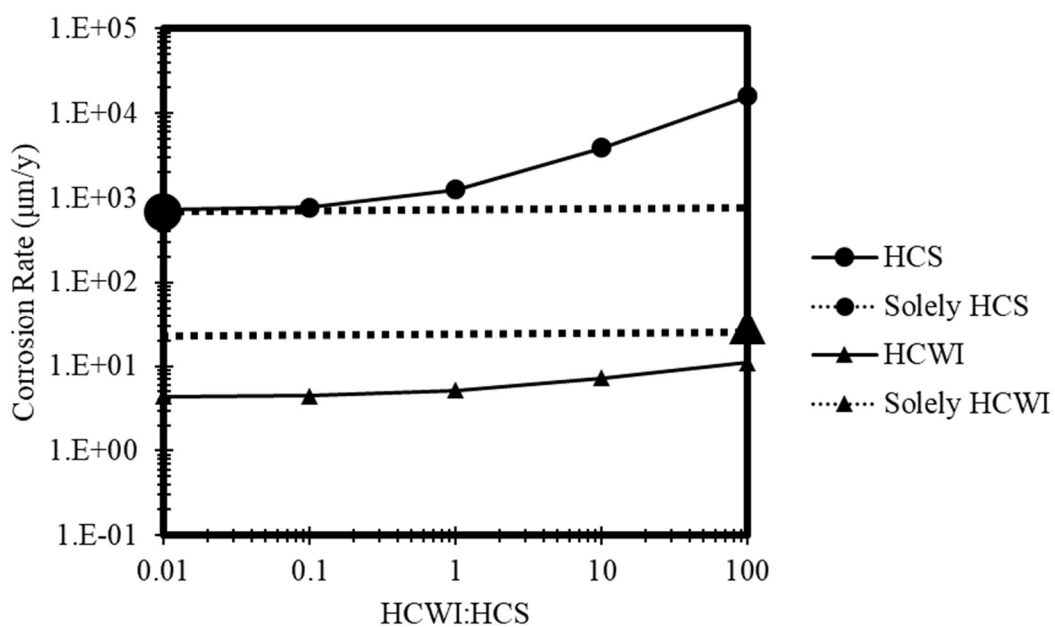
Figure 15. The effect of surface area ratios on couple corrosion rates in pH 5 aerated simulated mill water. The dashed lines represent the V_{corr} values for each material individually and the solid data sets represent coupled V_{corr} values.
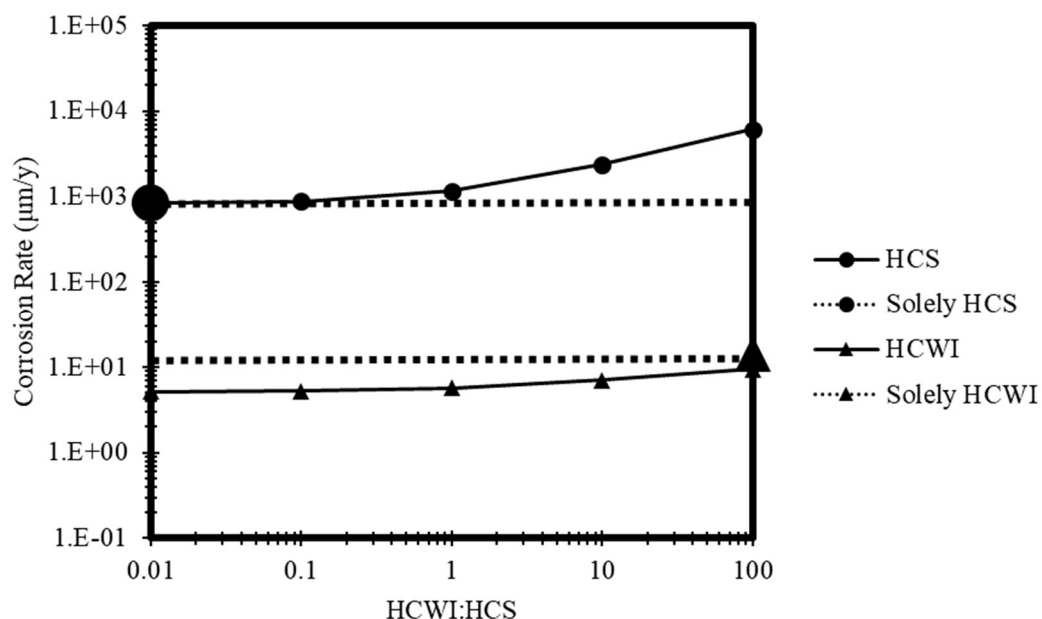
Figure 16. The effect of surface area ratios on couple corrosion rates in pH 9 aerated simulated mill water. The dashed lines represent the V_{corr} values for each material individually and the solid data sets represent coupled V_{corr} values.
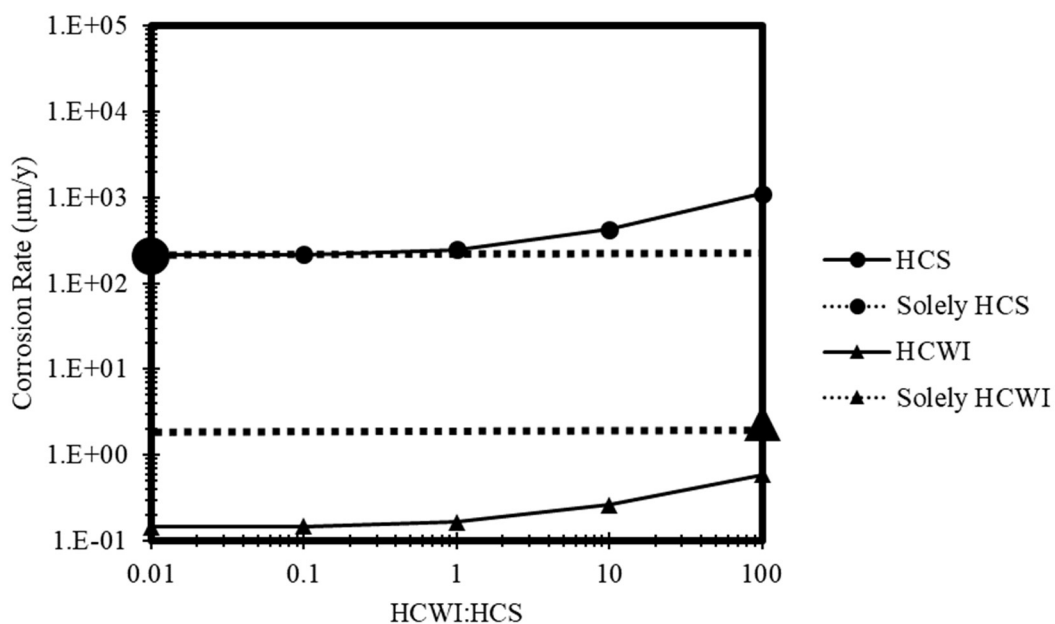
Figure 17. The effect of surface area ratios on couple corrosion rates in pH 11 aerated simulated mill water. The dashed lines represent the V_{corr} values for each material individually and the solid data sets represent coupled V_{corr} values.

Performing a surface area ratio analysis can be helpful with predicting corrosion rates for the coupled materials, but assumptions have been made that could adversely affect the use of these results. The first assumption is that the media will always be in electrical contact with each other. A ratio of 100 to 1 HCWI to HCS assumes that one HCS ball is in electrical contact with 100 HCWI balls of the same size, which may be unlikely. Another assumption is that electrical resistance does not affect the exchange of electrons. If electrons must travel though many other balls or there is significant resistance due to poor contact (e.g., ore particles between balls), the rate of electrons exchanging between the anode and cathode could change and alter the results. Grinding media may also interact with the mill liner and ore which could affect media corrosion rates [18]. Similar galvanic coupling mechanisms could be present if the electrochemical potentials of these materials are different.

Even so, the analysis of corrosion data for HCS and HCWI indicate that galvanic couple is certainly possible during MBWTs. The corrosion rate of HCWI can be significantly suppressed by even small amounts of HCS. Therefore, the impact of this phenomenon should be considered when economic decisions are made based on MBWT results.

5. CONCLUSIONS

Corrosion rates for modern grinding media have been measured as a function of mill water pH and chloride concentration. High chrome white iron (HCWI) was confirmed to have a higher electrochemical potential and lower corrosion rate than high

carbon steel (HCS) in all conditions examined. At lower pH levels, the corrosion rates were higher for both materials. Chloride concentrations from 1 to 4 grams per liter do not affect the corrosion rates measured by the electrochemical testing employed in this study. Galvanic coupling is possible between HCS and HCWI at all conditions tested. When coupled, HCWI's corrosion rate can decrease from 2 X to 93 X depending on conditions while increasing HCS's corrosion rate. While the possibility of galvanic coupling is confirmed, other factors can also affect the wear rate of the grinding media. This study indicates that the presence of HCS could impact the corrosion rate of HCWI and the host charge in a MBWT can affect the corrosion of media during the test.

REFERENCES

1. Isaacson, A. E. Effect of Sulfide Minerals on Ferrous Alloy Grinding Media Corrosion. U.S. Dept. of the Interior, Bureau of Mines, 1989.

2. Kawatra, S. K., et al. "Chapter 3.8: Grinding Circuit Design." *SME Mineral Processing & Extractive Metallurgy Handbook*, Society for Mining, Metallurgy & Exploration, Inc., Englewood, CO, 2019.

3. Aldrich, Chris. "Consumption of Steel Grinding Media in Mills – a Review." Minerals Engineering, vol. 49, 2013, pp. 77–91.

4. Adam, K., et al. "Electrochemical Aspects of Grinding Media-Mineral Interaction in Sulfide Ore Grinding." CORROSION, vol. 42, no. 8, 1986, pp. 440–447.

5. H. Abd-El-Kader, S.M. El-Raghy, Wear-corrosion mechanism of stainless steel in chloride media, Corrosion Science, Volume 26, Issue 8, 1986, Pages 647-653, ISSN 0010-938X

6. Greet, Christopher J. "A Protocol for Conducting and Analysing Plant Trials: Testing of High-Chrome Grinding Media for Improved Metallurgy." The Southern African Institute of Mining and Metallurgy, 2012

7. Vermeulen, L.A., and D.D. Howat. "Theories of Ball Wear and the Results of a Marked-Ball Test in Ball Milling." Journal of the Southern African Institute of Mining and Metallurgy, vol. 83, no. 8, 1 Aug. 1983.

8. Meulendyke, M.J., Moroz, P.J. & Smith, D.M. "Practical aspects of corrosion in the wear of grinding media." Mining, Metallurgy & Exploration 4, 72–77 (1987).

9. Meulendyke, M. J., and J. D. Purdue. "Wear of Grinding Media in the Mineral Processing Industry: An Overview - Mining, Metallurgy & Exploration." SpringerLink, Springer International Publishing, 1 Nov. 1989

10. Schneider, C. A., Rasband, W. S., & Eliceiri, K. W. (2012). NIH Image to ImageJ: 25 years of image analysis. Nature Methods, 9(7), 671–675. doi:10.1038/nmeth.2089

11. Tolley, William K., Ivan L. Nichols, and J. L. Huiatt. "Corrosion rates of grinding media in mill water." USBM Report of Investigations 8882 (1984).

12. Andrade, C., and C. Alonso. "Test Methods for on-Site Corrosion Rate Measurement of Steel Reinforcement in Concrete by Means of the Polarization Resistance Method - Materials and Structures." SpringerLink, Kluwer Academic Publishers.

13. Mansfeld, Florian. "Tafel Slopes and Corrosion Rates from Polarization Resistance Measurements." Corrosion, vol. 29, no. 10, 1973, pp. 397–402.

14. Feng, Weipeng, et al. "Methods of Accelerating Chloride-Induced Corrosion in Steel-Reinforced Concrete: A Comparative Review." Construction and Building Materials, vol. 289, 2021, p. 123165.

15. Lin, Bin, et al. "A Study on the Initiation of Pitting Corrosion in Carbon Steel in Chloride-Containing Media Using Scanning Electrochemical Probes." Electrochimica Acta, vol. 55, no. 22, 2010, pp. 6542–6545.

16. Lee, Siaw Foon, et al. "Pitting Corrosion Induced on High-Strength High Carbon Steel Wire in High Alkaline Deaerated Chloride Electrolyte." Nanotechnology Reviews, vol. 11, no. 1, 2022, pp. 973–986.

17. Qiu, Jie, et al. "Effect of Chloride on the Pitting Corrosion of Carbon Steel in Alkaline Solutions." Journal of The Electrochemical Society, vol. 169, no. 3, 2022, p. 031501.

18. Natarajan, K.A., and I. Iwasaki. "Electrochemical Aspects of Grinding Ball-Mineral Interactions in Ore Grinding." Key Engineering Materials, vol. 20-28, 1991, pp. 799–803.

19. ASTM Standard E2594-20, 2020, "Standard Test Method for Analysis of Nickel Alloys by Inductively Coupled Plasma Atomic Emission Spectrometry (Performance-based)," ASTM International, DOI: 10.1520/E2594-20.

20. ASTM Standard E1019-18, 2018, "Standard Test Methods for Determination of Carbon, Sulfur, Nitrogen, and Oxygen in Steel, Iron, Nickel, and Cobalt Alloys by Various Combustion and Inert Gas Fusion Techniques," ASTM International, DOI: 10.1520/E1019-18.

II. UNDERSTANDING CHARGE EFFECTS ON MARKED BALL WEAR RATES – A CORROSION STUDY: PART 2. THE IMPACT OF CHROMIUM CONTENT IN MEDIA AND DISSOLVED OXYGEN

John Bailey Fletcher and Michael S. Moats

Materials Research Center
Department of Materials Science and Engineering
Missouri University of Science and Technology
Rolla, MO, USA 65409

ABSTRACT

Grinding media consumption can be a costly aspect of milling. Marked ball wear tests (MBWT) can be used to assess the wear rates of various grinding media to help optimize costs. Corrosion, one component of wear, can be affected by many variables. Corrosion rates and corrosion potentials for modern high chromium white iron (HCWI) and high carbon steel (HCS) grinding media samples were obtained through electrochemical testing. In this study, the impact of chromium content in the grinding media and the dissolved oxygen in a simulated mill water solution on corrosion potentials and rates were examined. Increasing chromium content in HCWI above 15 weight percent increases the corrosion potential and decreases corrosion rate. Removing most of the oxygen from the solution lowers both the corrosion potential and corrosion rate of the materials tested. The electrochemical results were examined to model possible galvanic coupling effects on corrosion rates. Galvanic coupling between HCS and HCWI could cause differences in corrosion rates for almost all scenarios modeled. Based on the galvanic coupling analysis, MBWT results could be impacted by mixing HCWI and HCS

in a ball mill charge. This impact is predicted to be more significant when dissolved oxygen is present in the mill water and as the chromium content of HCWI is above 15 weight percent.

1. INTRODUCTION

Grinding media consumption in steel ball mills can be expensive for mining operations [1]. In wet milling operations, grinding media wears by abrasion, impact, and corrosion [2]. Selecting a grinding media material that has the best overall wear performance in relation to its price is an important economic decision for operators [3, 4]. Commonly, a marked ball wear test (MBWT) [5] is used to measure wear rates of different media at the same time. However, the impact of possible galvanic interactions between dissimilar media has been neglected in interpreting MBWT results to date.

In Part 1 of this study, corrosion potentials and rates were shown to be affected by the pH of mill water for both high carbon steel (HCS) and high chrome white iron (HCWI). Chloride ion concentration from one to four grams per liter did not impact the corrosion measurements. The electrochemical measurements indicated that galvanic coupling between HCS and HCWI was theoretically possible at all conditions examined and could significantly impact the corrosion rates of materials in a MBWT or in a mixed media charge.

Previous researchers have also shown that corrosion potentials and rates can be impacted the chromium composition of the grinding media [6, 7, 8]. The addition of chromium to steel or cast irons is well known as a method to improve the corrosion

resistance of the materials. Chromium creates a thin passivation layer that slows the corrosion of the material. Stainless steels (similar chromium content as HCWI) need a minimum of 10.5 wt.% Cr to form this passivation layer [9]. Higher chromium content and chromium carbide volume fractions have been shown to increase corrosion resistance [6, 7, 8] as well as the price of the material [10].

Another factor that could change the corrosion characteristics of grinding media is the availability of oxygen in the milling water [11, 12]. Ball mills can have different levels of dissolved oxygen based on their design and operation. While oxygen seems to be readily available in many circumstances, some systems could have reactions that consume available oxygen. The main cathodic reaction in grinding media corrosion is believed to be oxygen reduction [13]. Thus, changing the amount of oxygen present in the system can directly affect the cathodic reaction, which would also change the corrosion potential and rate [11, 12]. Mild steels [12], stainless steels [12], and hypersteels [14] corrode faster when dissolved oxygen levels are increased. Increasing the amount of oxygen also increases the galvanic interactions between grinding media and sulfide minerals [14, 15, 16].

As shown in Part 1, the galvanic interaction between dissimilar grinding media during a MBWT could impact the corrosion rates enough to misrepresent wear rates of the media. Industrial studies have found that when HCWI is added to a HCS charge, the wear rate of HCWI is two to three times less than when added to a HCWI charge [17, 18]. Part 1 elucidated the effects of galvanic coupling on the corrosion rates for limited HCS and HCWI media samples in simulated mill water at various pH and chloride concentrations. This study (Part 2) performs galvanic coupling analyses on HCS and

HCWI media with various chromium content and media in simulated mill water at two dissolved oxygen concentrations.

2. METHODS

The experimental testing procedure to determine corrosion potentials (E_{corr}) and corrosion current (i_{corr}) of different grinding materials was provided in detail in Part 1 and was similar to a 1984 U.S. Bureau of Mines study [13]. Eleven commercial grinding media samples were provided by an industrial supplier. Specimens from each sample were fabricated into electrodes for electrochemical testing. Chromium composition ranged from 0.32 to 27.9 weight percent for high carbon steels and white irons. Sample compositions were determined by a commercial laboratory and summarized in Table 1.

Table 1. Chemical compositions for grinding media samples. Compositions gathered from inductively coupled plasma (ICP) methods (ASTM E2594-20 modified [23] and ASTM E1019-18 [24]) performed by a commercial laboratory.

Material	HCS				HCWI						
Weight %	A	B	C	D	E	F	G	H	I	J	K
Chromium	0.32	0.32	1.98	2.00	14.3	14.4	16.0	23.2	26.4	27.6	27.9
Carbon	1.07	1.01	0.86	0.87	2.89	2.77	2.90	2.57	2.62	2.60	2.57
Manganese	0.83	0.83	0.38	0.39	0.60	1.16	0.84	0.32	0.31	0.33	0.31
Silicon	0.15	0.15	0.28	0.28	2.11	0.96	0.82	1.09	1.58	1.12	1.62

All samples were electrochemically tested in four different environments, which are summarized in Table 2. The electrolyte was simulated mill water as described in Part

1. 10 molar sodium hydroxide was added to the simulated mill water adjust the pH and avoid excessive dilution of dissolved salts.

Table 2. Experimental testing environments.

Environment	pH	Gas Sparge
1	7	Air
2	7	Nitrogen
3	11	Air
4	11	Nitrogen

Air and nitrogen sparging were performed by bubbling compressed air or nitrogen into the electrolyte prior to testing to control the dissolved oxygen concentration and simulate two extremes possible during milling. Figure 1 shows the average dissolved oxygen level vs. sparging time from three separate experiments for both air sparging and nitrogen sparging. After 30 minutes, the oxygen content raised to 6.58 from 5.23 mg L^{-1} for an air sparged experiment. For nitrogen sparged experiments, the oxygen content lowered to 0.06 milligrams per liter. All systems were sparged for 30 minutes before electrochemical testing began to achieve a steady concentration of dissolved oxygen. During the experiments, the sparging tube was placed above the solution but remained within the confined cell to create a blanket over the top of the solution.

Following corrosion testing, each media sample was ground and polished using ASTM standard E3-11 for microstructural examination [19]. Silicon carbide polishing papers and diamond paste suspensions were used to produce a mirror finish. The samples' surfaces were etched with 2% nital, picric acid, and Adler's etchant diluted in

de-ionized water at a volume ratio of 1:1 depending on the chromium content of the sample.
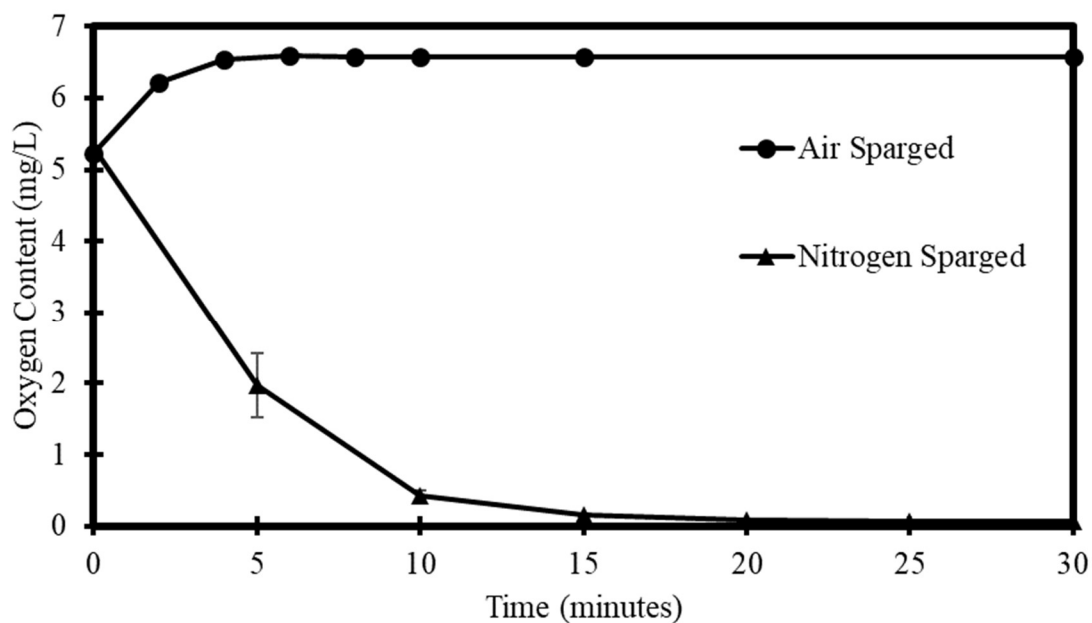
Figure 1. Dissolved oxygen content in simulated mill water over time for air and nitrogen sparging before experimentation.

Samples A, E, and K were used to examine experimental repeatability of the corrosion tests. These three samples were selected to examine the full range chromium content tested and were tested five separate times in environment 1 to measure experimental variability. This variability is shown as error bars in plots. All other corrosion experiments were performed once.

3. RESULTS AND DISCUSSION

To find the corrosion potential (E_{corr}), corrosion current density (i_{corr}), and Tafel slopes for each grinding media sample, electrochemical testing was performed with the media sample as the working electrode. Figure 2 is a schematic representation of the result of a potentiodynamic scan and is often called a polarization curve, or Evan's diagram. The anodic branch is more positive than the E_{corr} and represents the oxidation reaction of the corrosion event. This is the metal dissolution reaction. The cathodic branch is more negative than the E_{corr} and represents the reduction reaction (in the corrosion of grinding media, this is most likely to be oxygen reduction [13]). When the two reactions are occurring at the same rate, the potential is the E_{corr} value. The intersection of the E_{corr} and the Tafel slopes (linear portion of each reaction branch) is an i_{corr} value. Because the i_{corr} value is directly related to the corrosion rate of the material, changing the E_{corr} or the Tafel slopes will affect the corrosion rate (V_{corr}). The relationship between i_{corr} and V_{corr} is shown in Equation 1. 1.16×10^7 is a constant used to represent corrosion in an iron matrix [20]. The Tafel slopes are determined by selecting the linear portion of data at least 50 mV away from the E_{corr} (the high field approximation of the Butler Volmer equation). A further explanation on how the Tafel slopes were determined was presented previously in Part 1.

$$V_{corr} \left(\frac{\mu m}{y} \right) = 1.16 * 10^7 i_{corr} \left(\frac{A}{cm^2} \right) \tag{1}$$

The experimental results of selected grinding media samples in aerated simulated mill water at pH 7 are displayed in Figure 3. Samples A (a HCS) and E (a HCWI with 14.3 wt% Cr) show very similar results. The other three HCWI samples (H, I, and K)

exhibit higher E_{corr} values and decreased i_{corr} values compared to samples A and E. The

scan results show the general trend that when Cr content increases above a certain

percentage, E_{corr} values increase and i_{corr} values decrease (V_{corr} also decrease).
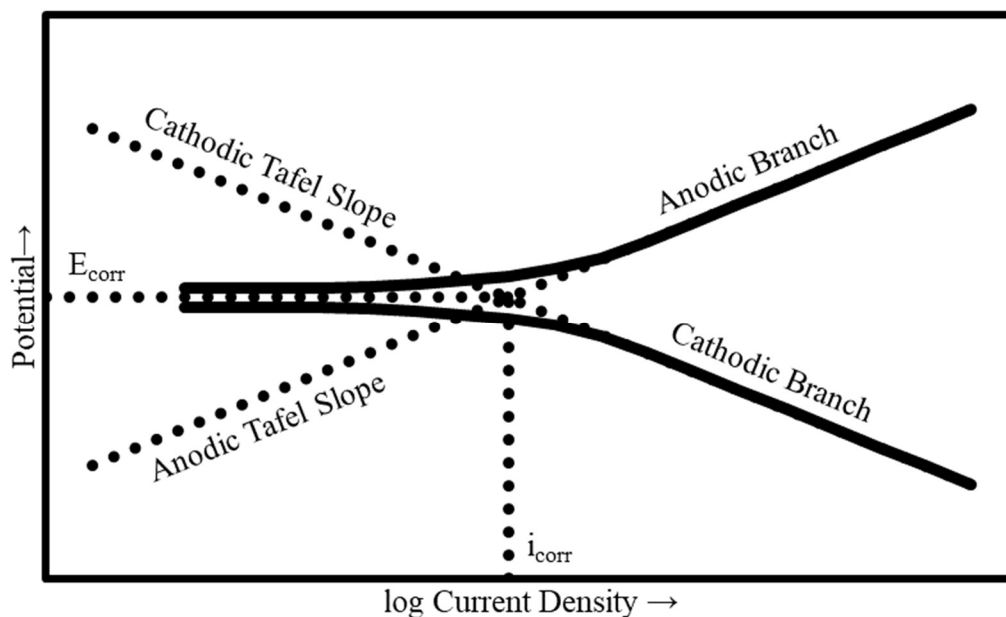
Figure 2. Theoretical result of a potentiodynamic scan. Shown are how the E_{corr}, i_{corr}, and Tafel slopes are determined.

The effects of Cr concentration and dissolved oxygen on E_{corr} and V_{corr} values in

simulated mill water with a pH of 7 are displayed in Figures 4 and 5, respectively. E_{corr}

increases by ca. 0.2 V in an air sparged electrolyte when the chromium content of the

media is greater than 15 wt%. Corrosion rates decrease approximately two orders of

magnitude once the chromium content is above 15 wt% Cr for the HCWI samples.
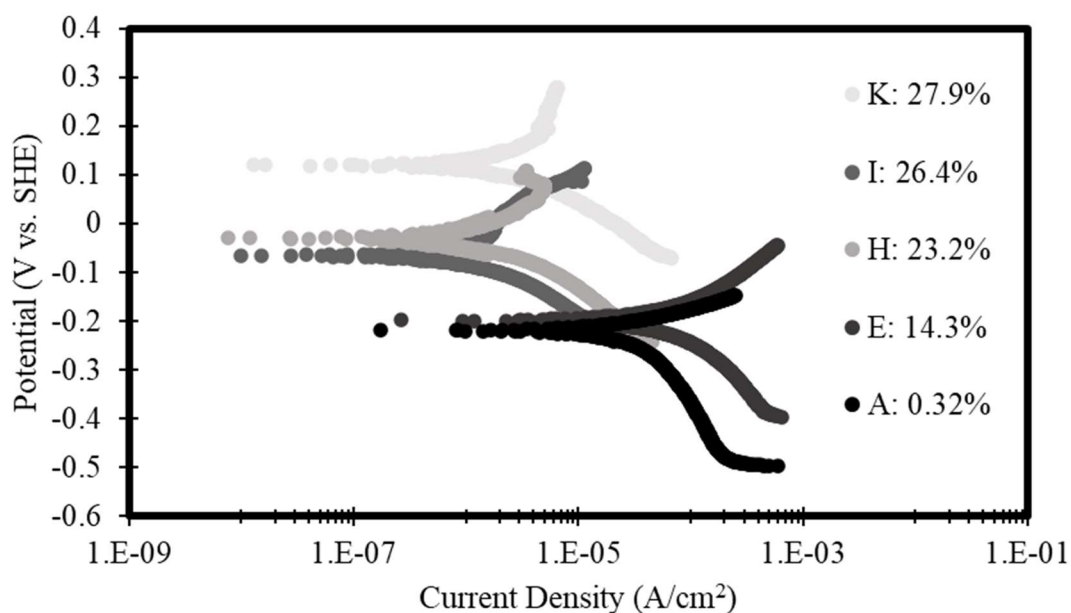
Figure 3. Potentiodynamic scan results for a HCS sample (A) and four HCWI samples with a range of chromium content (E, H, I, K) in aerated simulated mill water at pH 7.
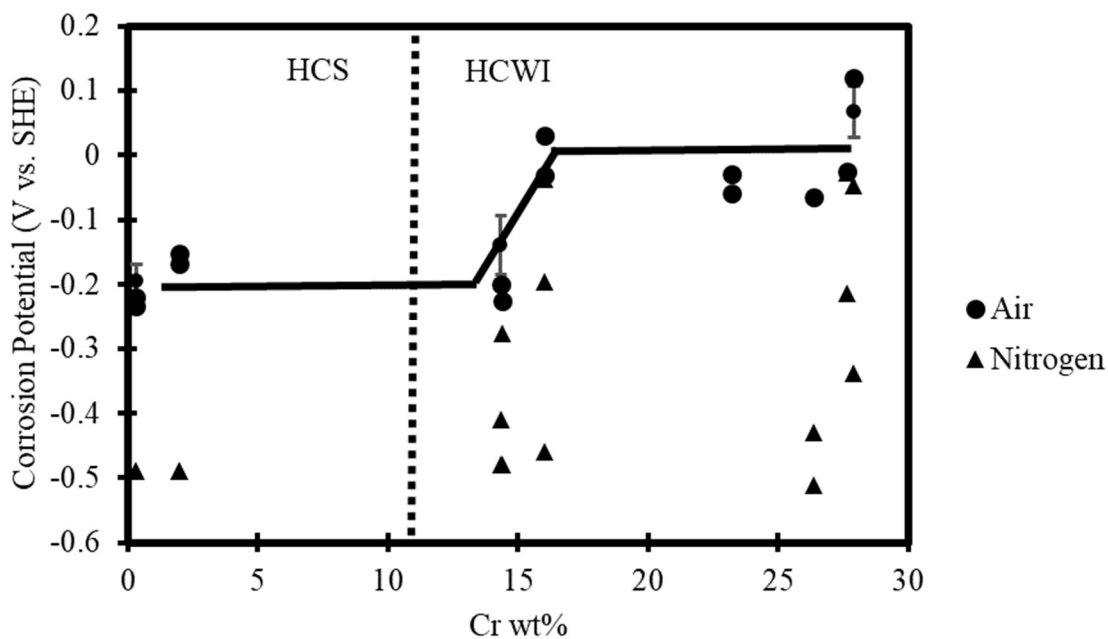
Figure 4. Corrosion potential plotted versus chromium weight percent for both air and nitrogen environments at a pH of 7. Three data points have error bars showing +/- one standard deviation from five replicates.
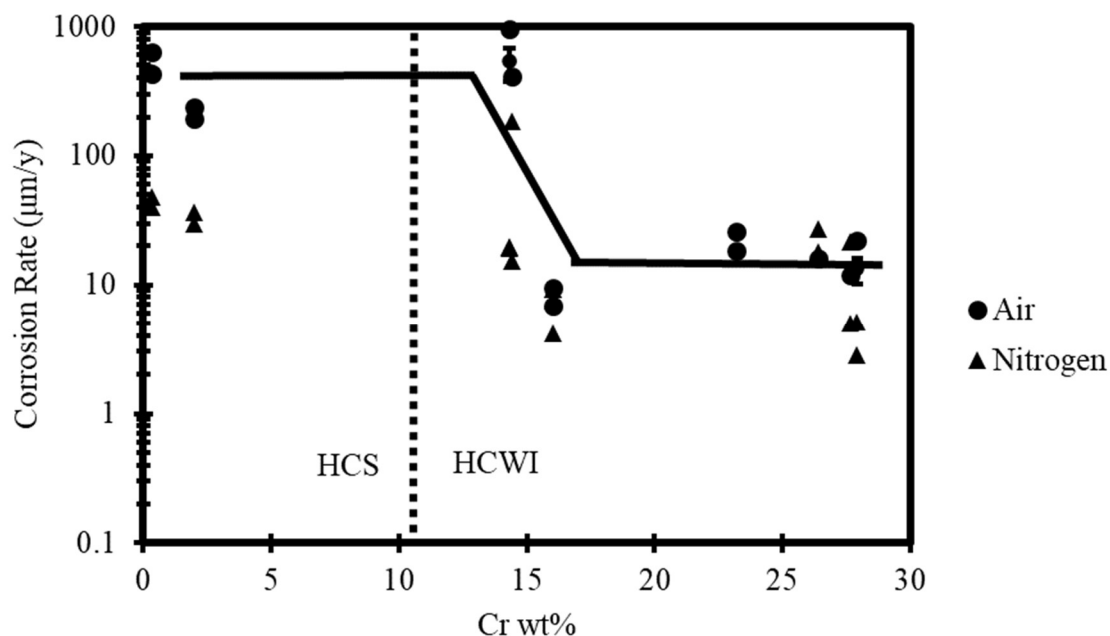
Figure 5. Corrosion rates versus chromium weight precent in simulated mill water at pH 7. Three data points have error bars showing +/- one standard deviation from five replicates.

The effects of chromium content on E_{corr} and V_{corr} values in a pH 11 simulated mill water are provided in Figures 6 and 7, respectively. E_{corr} values at pH 11 display a similar increase with increasing Cr content as at pH 7. Figure 7 again shows a two-order magnitude decrease in corrosion rate when the chromium content of HCWI is greater than 15 wt%.

Figures 4 and 6 demonstrate that E_{corr} increases once a threshold of chromium is achieved and agrees with previous studies [6, 8]. The amount of chromium carbides in the microstructure are known to affect the corrosion rate of high chrome white iron [6]. When the chromium carbide forms, it can deplete the chromium present in the iron matrix and result in intergranular corrosion [21].
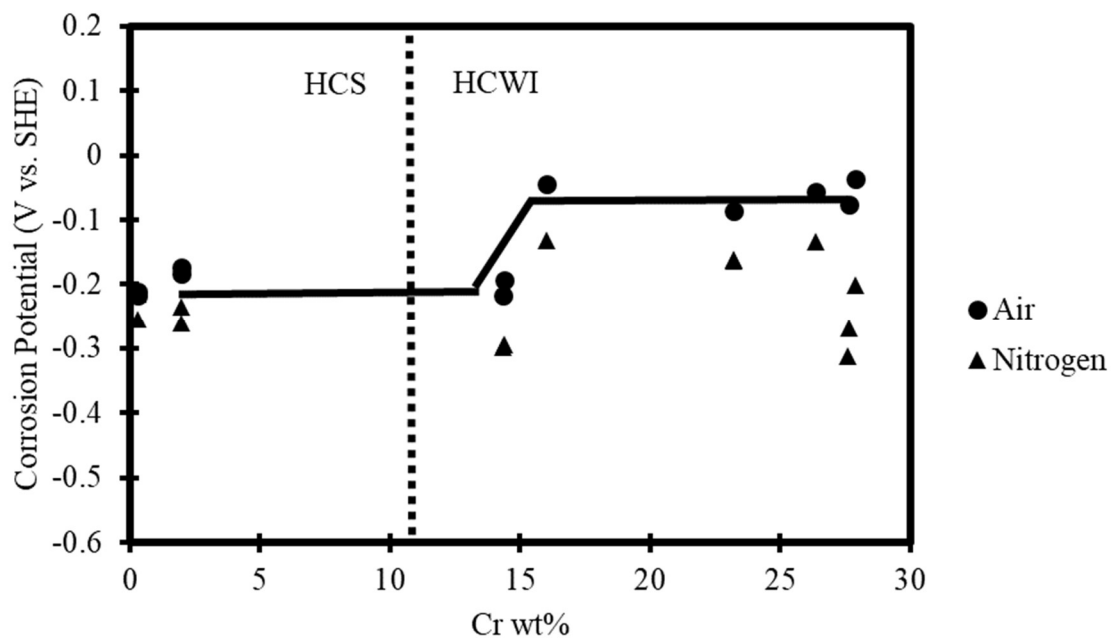
Figure 6. E$_{corr}$ change with chromium weight percent for both air and nitrogen environments at a pH of 11.
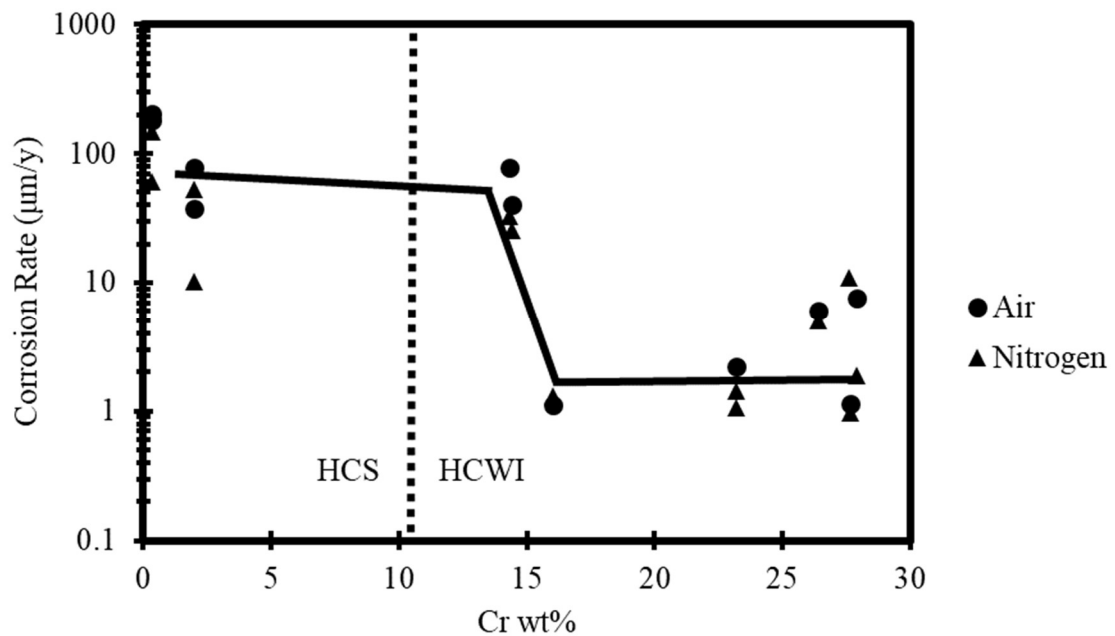
Figure 7. V$_{corr}$ at different chromium weight precents for the same experiments shown in Figure 6.

Figures 4 and 6 contain the results of the experimental repeatability study. Samples A, E, and K (0.32, 14.3, and 27.9 Cr wt%) were tested separately in the same environment five times. Their average E_{corr} and V_{corr} values display error bars that indicate the standard deviation of the five experiments. Sample E displayed the most variation and this is most likely due its chromium content being near 15 Cr wt%.

HCWI will form a passivation layer that will lower the corrosion rate [22], but this layer is believed to be removed during grinding [13]. Passivation can appear as a decrease or plateau in current density with increasing potential during a potentiodynamic scan [2], which can be seen near the end of the anodic branches of sample H and K in Figure 3. While some passivation has occurred, Part 1 has shown that the experimental method used minimized the formation of the passive layer on the surface which allowed for an accurate determination of E_{corr}, i_{corr} and the anodic Tafel slop. The combination of amount of chromium carbide and chromium oxide layer (passivation layer) could result in noticeable corrosion changes in HCWI media with a chromium content greater than 15 wt% Cr for these specific materials.

The effect of adding more Cr (0.32% vs. 1.99%) to HCS on corrosion can be observed by examining the results of samples A, B, C, and D. Increasing the chromium content modestly did not alter the E_{corr} but did appear to lower the corrosion rates by 100-250 μm y^{-1} for the pH levels tested. The decrease in corrosion rate is much smaller compared to the 900-1000 μm y^{-1} change that occurs when chromium content of HCWI is greater than 15 wt%. Since grinding media wear rates are a function of impact, abrasion, and corrosion [2], it is unclear if reducing the corrosion rate by 100-250 μm y^{-1} is worth the cost of increasing the chromium in HCS to 2 wt%.

The impact of removing most of the dissolved oxygen from the testing solution by nitrogen sparging on corrosion of grinding media is shown in Figures 4-7. The nitrogen sparged experiments exhibited significant variation. While the exact cause of this variation is unknown, it is believed that ingression of oxygen during the experiment may have resulted in higher than anticipated dissolved oxygen in the solution. While the scatter is significant, it is believed that removing most of the dissolved oxygen generally lowered the corrosion potential at pH 7 and 11 (see Figures 4 and 6) and decreased the corrosion rate (see Figures 5 and 7). These results confirm previous findings with other steels [12, 14]. Removing oxygen from the electrolyte could have changed the cathodic reaction from oxygen reduction to hydrogen evolution, but more experimentation is needed to confirm if the underlying cathodic reaction changed.

Optical micrographs of samples A, C, E, G, I, and K are provided in Figure 8. These samples were selected to examine the impact of chromium on microstructure. The HCS samples, A and C were etched with 2% nital. Sample E has a higher chromium content and could not be etched with 2% nital, so picric acid was used as the etchant. G, I, and K were etched with Adler's etchant diluted in de-ionized water at a 1:1 volume ratio as picric acid was not effective. Qualitatively, the aggressiveness of the etchant used corresponds to the corrosion resistance measured by electrochemical methods, which provides some confirmation to these results.
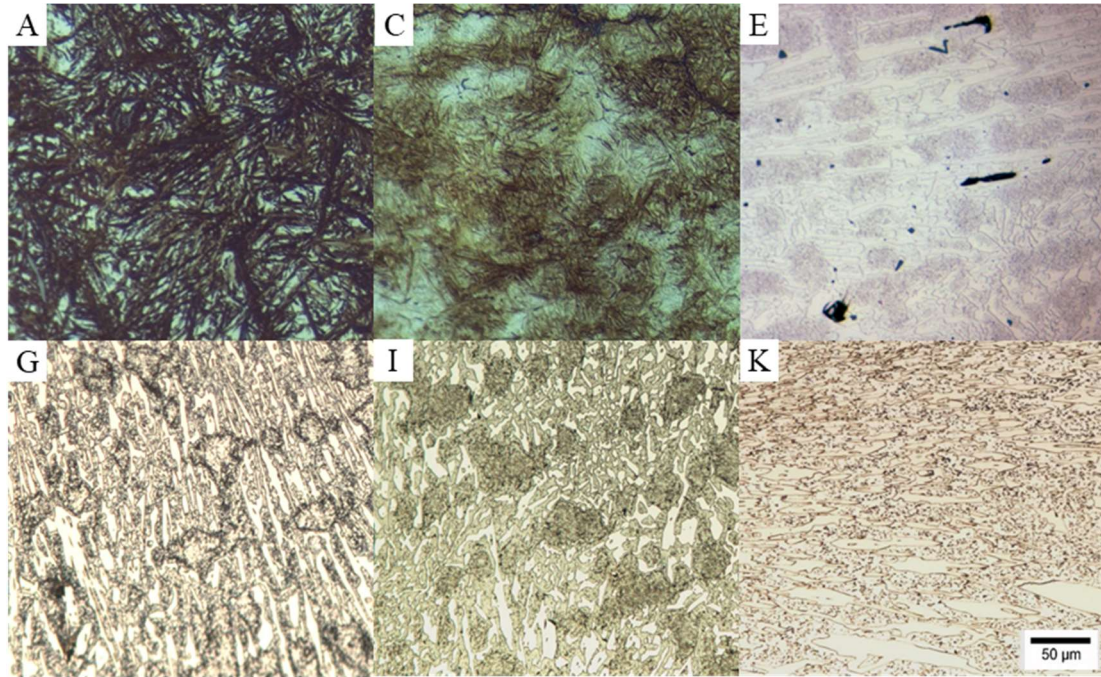
Figure 8. Micrographs of selected samples. A: 0.32 wt% Cr HCS etched with 2% nital, C: 2.0% wt. Cr HCS etched with 2% nital, E: 14.3 wt% Cr etched with picric acid, G: 16.0 wt% Cr etched with picric acid, I: 26.4 wt% Cr etched with 50% Adler's Etchant, K: 27.9 wt% Cr etched with 50% Adler's Etchant.

Samples A and C are forged high carbon steel. Their micrographs in Figure 8 display retained austenite (lighter color) and martensite (dark areas). A and C appear to have similar microstructures because of their similar compositions and presumed processing method. Samples E, G, I, and K are all casted HCWI. The white areas in these images are carbides. The darker sections that appear to contain dendrites are a mixture of martensite and retained austenite. Sample E has a chromium content less than the 15 wt% threshold. This sample displays depletion in the iron matrix near the grain boundaries that would lead to corrosion susceptibility. Above the 15 Cr wt% threshold, the iron matrix is does not show depletion around the grain boundaries. Another conclusion from the micrographs is that the grain size of sample K is much finer than the other HCWI

samples. The fine grain structure does not seem to affect the corrosion rate under the conditions tested.

4. GALVANIC COUPLING ANALYSIS

In Part 1 of this study, galvanic coupling analysis between HCS and HCWI was described in detail. In this study, each HCWI sample was compared to Sample A to determine the impact of galvanic coupling on corrosion rate as a function of surface area ratio. Figures 9-14 display the effect of changing the surface area ratios of different HCWI samples and one HCS (Sample A) in aerated simulated mill water at pH 7 on their corrosion rates. The dashed lines represent the corrosion rate of each material when they are not coupled, and the solid black data points and lines represent the corrosion rates of each material when HCWI and HCS are in a galvanic couple.

Figure 9 displays the analysis results for sample F (14.4% Cr). This sample has a similar corrosion rate and corrosion potential to HCS sample A. Because these two samples have similar corrosion values, the coupled corrosion rates are not different than the individual corrosion rates. This scenario shows that galvanic coupling would not affect the corrosion rates because the two samples have similar values.

The coupled galvanic corrosion rates for different surface area ratios of samples A and H (23.2 wt% Cr) in aerated simulated mill water at pH 7 are provided in Figure 10. Raising the chromium content decreased the V_{corr} values for the HCWI sample and has increased the effects of galvanic coupling between the two materials. Having a mixed charge with a surface area ratio of 1 HCWI to 1 HCS in this scenario shows the HCWI

coupled V_{corr} is 80% less than the individual HCWI V_{corr}. At this ratio, the HCS coupled

V_{corr} increases by 60% as compared to HCS's individual V_{corr}. Galvanic coupling in a

mixed charge of these materials could impact MBWT results.
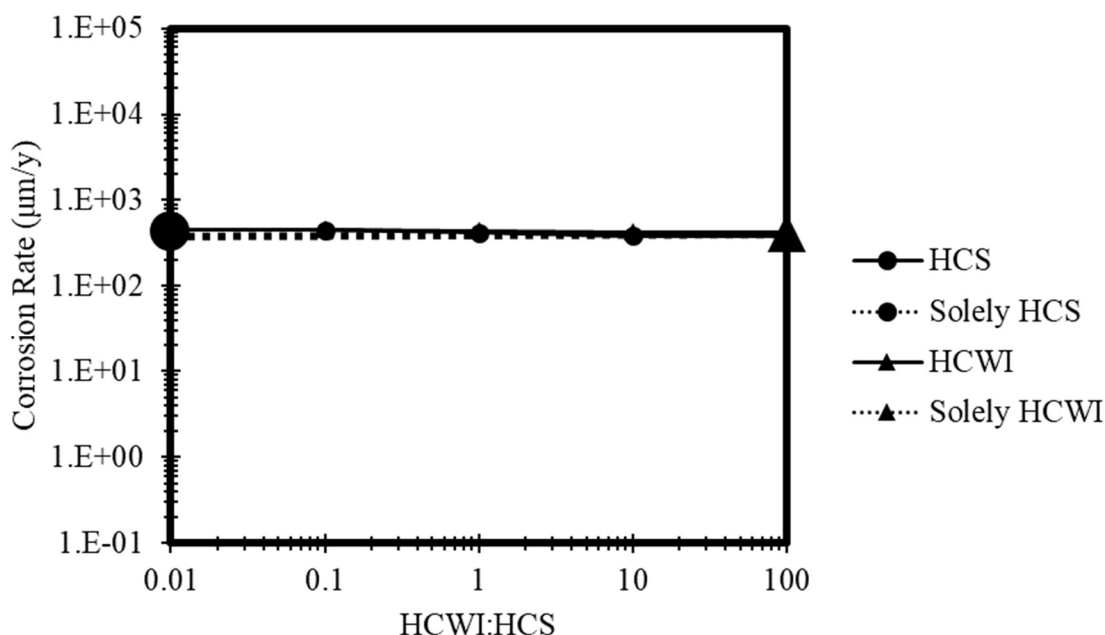
Figure 9. The effect of surface area ratios (HCWI:HCS) on galvanic coupled corrosion rates between sample F (14.4 wt% Cr HCWI) and sample A (a HCS) in aerated simulated mill water at pH 7. The dashed lines represent the V_{corr} values for each material individually and the solid data sets represent coupled V_{corr} values.

The coupled galvanic corrosion rates for different surface area ratios of samples A

and K (27.9 wt% Cr) in aerated simulated mill water at pH 7 are provided in Figure 11.

The 27.9 wt% Cr HCWI increases the effects of galvanic coupling on corrosion rates. In

a mixed charge with a surface area ratio of 1 HCWI to 1 HCS, the HCWI coupled V_{corr} is

2.4% of the individual HCWI V_{corr} value, while the HCS coupled V_{corr} increases by 900%

as compared to the individual HCS V_{corr} value. Hence, galvanic coupling in a mixed

charge with these two materials at these conditions could have a significant impact on

MBWTs.
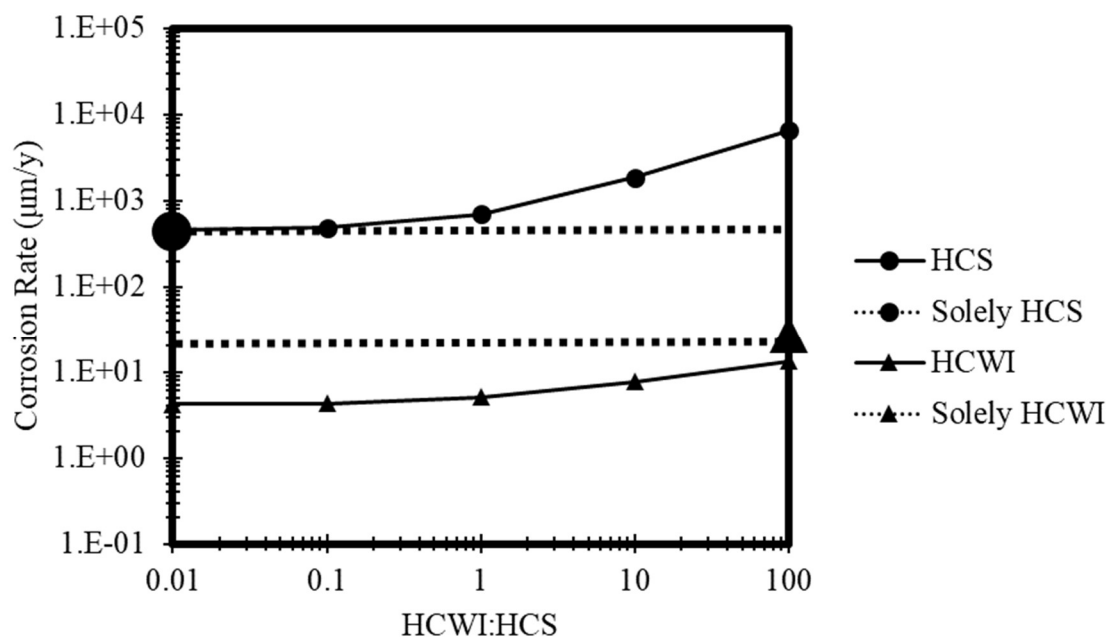
Figure 10. The effect of surface area ratios (HCWI:HCS) on galvanic coupled corrosion rates between sample H (23.2 wt% Cr HCWI) and sample A (a HCS) in aerated simulated mill water at pH 7. The dashed lines represent the V_{corr} values for each material individually and the solid data sets represent coupled V_{corr} values.

The galvanic coupling of samples F, H and K with Sample A were also examined

in aerated simulate mill water at pH 11. Figure 12 displays results of the galvanic

coupling analysis for Sample F (14.4% Cr) with Sample A. At pH 11, the corrosion

values of Samples A and F are different enough to change the corrosion rates when

coupled, although the differences are relatively small. At a 1 HCWI to 1 HCS ratio,

HCWI's coupled V_{corr} decreases 38% compared to its individual V_{corr} value. HCS's

coupled V_{corr} value increases by 20% compared to HCS's individual V_{corr} value.

Interestingly at a pH 11, galvanic coupling may slightly impact MBWT testing if these

materials are present which is different than at a pH 7. This highlights that water

conditions can impact the ability to interpret whether galvanic couplings might affect

MBWT results.
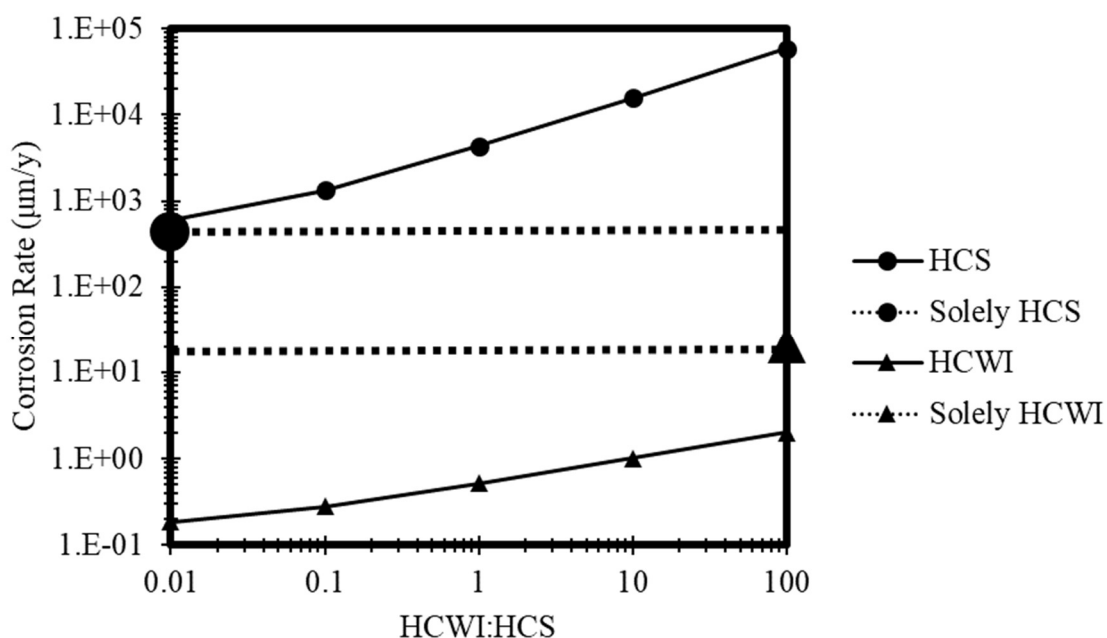
Figure 11. The effect of surface area ratios (HCWI:HCS) on galvanic coupled corrosion
rates between sample K (27.9 wt% Cr HCWI) and sample A (a HCS) in aerated
simulated mill water at pH 7. The dashed lines represent the V_{corr} values for each material
individually and the solid data sets represent coupled V_{corr} values.

The coupled galvanic corrosion rates for different surface area ratios of samples A

and H (23.2 wt% Cr) in aerated simulated mill water at pH 11 are shown in Figure 13.

The HCS's coupled V_{corr} is the same as the HCS's individual V_{corr} for low HCWI to HCS

ratios. At a 1 HCWI to 1 HCS ratio, HCS's V_{corr} does not change while HCWI's coupled

V_{corr} decreases by 93% as compared to HCWI's individual V_{corr}. This analysis indicates

that MBWT results could be compromised for HCWI samples at these conditions.
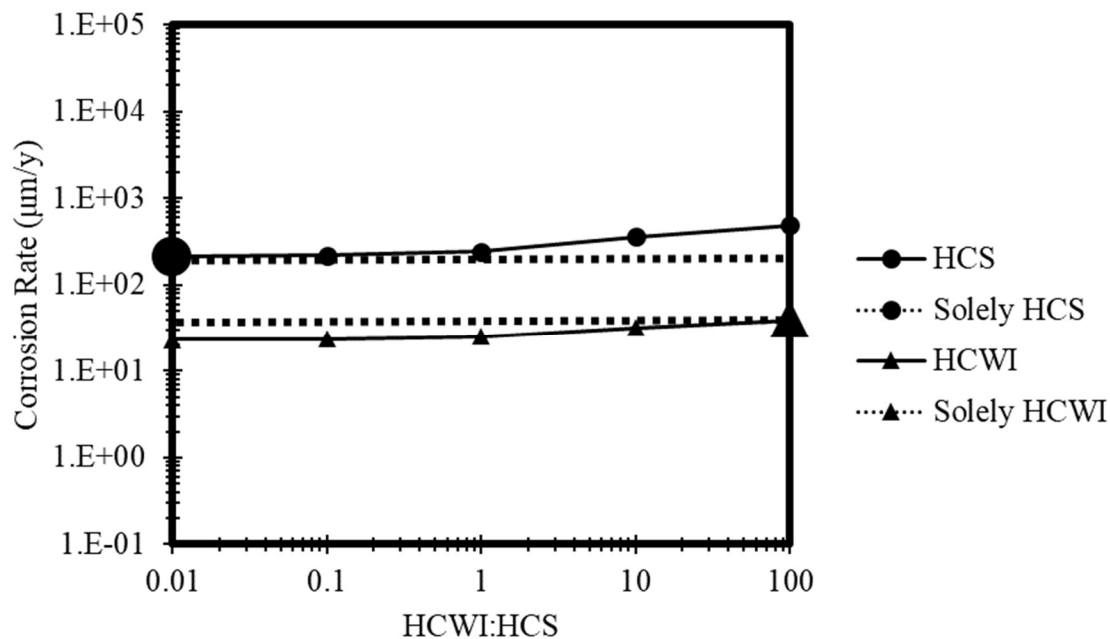
Figure 12. The effect of surface area ratios (HCWI:HCS) on galvanic coupled corrosion rates between sample F (14.4 wt% Cr HCWI) and sample A (a HCS) in aerated simulated mill water at pH 11. The dashed lines represent the V_{corr} values for each material individually and the solid data sets represent coupled V_{corr} values.

Finally, Figure 14 examines the galvanic couple of 27.9% Cr HCWI (H) with a

HCS (A) at pH 11. At a 1 HCWI to 1 HCS surface area ratio, the HCWI's coupled V_{corr}

decreasing 67% and HCS's coupled V_{corr} increases by 80%. While the results indicate

galvanic couple could impact MBWT tests with these materials in contact with each

other, the impact is less at pH 11 than pH 7.
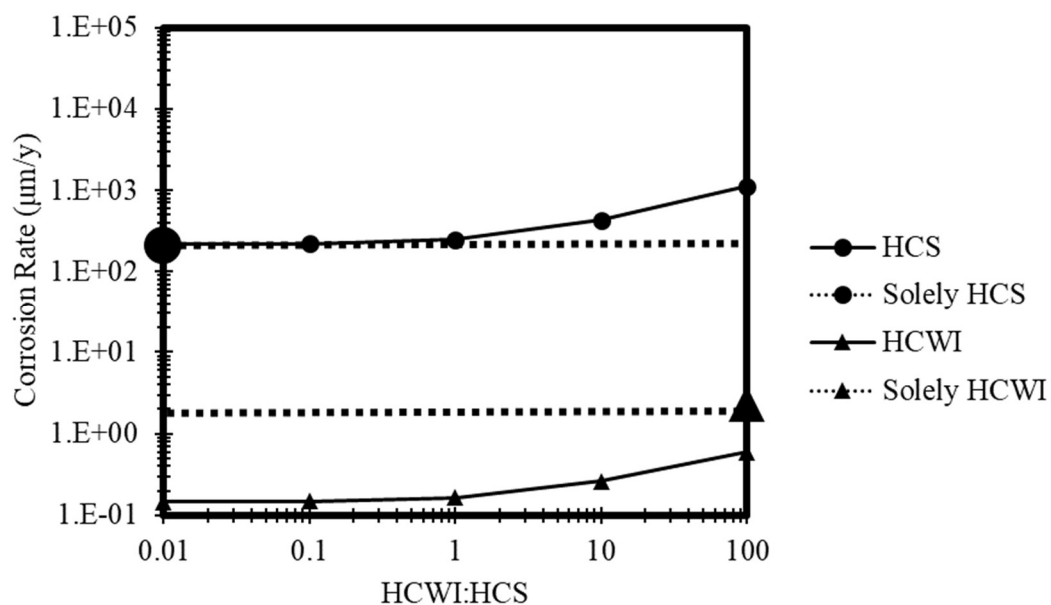
Figure 13. The effect of surface area ratios (HCWI:HCS) on galvanic coupled corrosion rates between sample H (23.2 wt% Cr HCWI) and sample A (a HCS) in aerated simulated mill water at pH 11. The dashed lines represent the V_{corr} values for each material individually and the solid data sets represent coupled V_{corr} values.
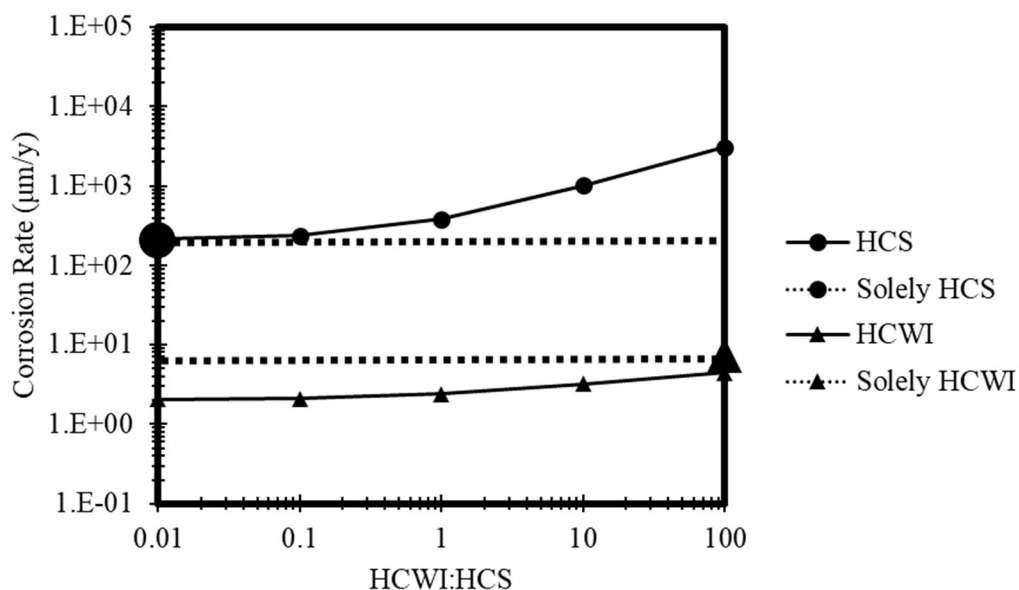
Figure 14. The effect of surface area ratios (HCWI:HCS) on galvanic coupled corrosion rates between sample K (27.9 wt% Cr HCWI) and sample A (a HCS) in aerated simulated mill water at pH 11. The dashed lines represent the V_{corr} values for each material individually and the solid data sets represent coupled V_{corr} values.

Galvanic coupling analyses were not performed for the nitrogen sparged results due to the scatter in the experimental results. Some results indicate that HCS and HCWI samples have little to no difference in E_{corr} values and thus galvanic coupling would not affect their corrosion rates. In these cases, the surface area ratio analysis graphs would be like Figure 9. Other results display E_{corr} differences that would result in galvanic coupling and affect the corrosion rates of both HCS and HCWI, but the results are scattered and difficult judge.

5. CONCLUSIONS

Corrosion of grinding media in ball mills can be affected by several variables. The impact of chromium content of grinding media and dissolved oxygen in the solution on corrosion potential and rate was examined in simulated mill water at pH 7 and 11. Increasing the chromium content of HCWI above 15 wt% Cr increases the corrosion potential (E_{corr}) and decreases the corrosion rate (V_{corr}). Adding 2 wt% Cr to HCS resulted in a minimal corrosion rate decrease. A higher concentration of dissolved oxygen in the electrolyte generally increases E_{corr} and V_{corr} values for the grinding media tested. For samples with different corrosion potentials, galvanic coupling is possible and can impact the predicted corrosion rates during a MBWT. The magnitude of this impact is difficult to obtain from this work, but corrosion rates were altered by 1-2 orders of magnitude by galvanic coupling in this analysis. Thus, it appears that MBWT results can

be affected by galvanic coupling and lead to misrepresentation of wear rates of grinding media.

REFERENCES

1. Iwasaki, I., et al. "Nature of Corrosive and Abrasive Wear in Ball Mill Grinding." International Journal of Mineral Processing, vol. 22, no. 1-4, 1988, pp. 345–360.

2. Isaacson, A. E. Effect of Sulfide Minerals on Ferrous Alloy Grinding Media Corrosion. U.S. Dept. of the Interior, Bureau of Mines, 1989

3. Aldrich, Chris. "Consumption of Steel Grinding Media in Mills – a Review." Minerals Engineering, vol. 49, 2013, pp. 77–91.

4. Le Bozec, N., et al. "Influence of Stainless Steel Surface Treatment on the Oxygen Reduction Reaction in Seawater." Corrosion Science, vol. 43, no. 4, 2001, pp. 765–786.

5. Vermeulen, L.A., and D.D. Howat. "Theories of Ball Wear and the Results of a Marked-Ball Test in Ball Milling." Journal of the Southern African Institute of Mining and Metallurgy, vol. 83, no. 8, 1 Aug. 1983.

6. Zumelzu, E, et al. "Wear and Corrosion Behaviour of High-Chromium (14–30% CR) Cast Iron Alloys." Journal of Materials Processing Technology, vol. 128, no. 1-3, 2002, pp. 250–255.

7. Lu, Baotong, et al. "Corrosion and Wear Resistance of Chrome White Irons—a Correlation to Their Composition and Microstructure." Metallurgical and Materials Transactions A, vol. 37, no. 10, 2006, pp. 3029–3038.

8. Tang, X.H., et al. "Variations in Microstructure of High Chromium Cast Irons and Resultant Changes in Resistance to Wear, Corrosion and Corrosive Wear." Wear, vol. 267, no. 1-4, 2009, pp. 116–121.

9. Kerber, Susan J., and John Tverberg. "STAINLESS STEEL." Advanced Materials & Processes, vol. 158, no. 5, Nov. 2000, p. 33. Gale Academic OneFile.

10. Gundewar, C.S., et al. "Studies on Ball Wear in the Grinding of Kudremukh Hematite-Magnetite Ore." Minerals Engineering, vol. 3, no. 1-2, 1990, pp. 207–220.

11. Wang, Jiamei, et al. "Effects of Corrosion Potential, Dissolved Oxygen, and Chloride on the Stress Corrosion Cracking Susceptibility of a 316ng Stainless Steel Weld Joint." CORROSION, vol. 75, no. 8, 2019, pp. 946–959.

12. Tait, W. S. "Effect of Physical Parameters on the Pitting Corrosion of Mild Steel in Low Total Dissolved Solids, Oxygen Bearing Waters: A Nonpassivating Metal/Environment System." Corrosion, vol. 35, no. 7, 1979, pp. 296–300.

13. Tolley, William K., Ivan L. Nichols, and J. L. Huiatt. "Corrosion rates of grinding media in mill water." USBM Report of Investigations 8882 (1984).

14. Vathsala, and K.A. Natarajan. "Some Electrochemical Aspects of Grinding Media Corrosion and Sphalerite Flotation." International Journal of Mineral Processing, vol. 26, no. 3-4, 1989, pp. 193–203.

15. Huang, Guozhi, et al. "Galvanic Interaction between Grinding Media and Arsenopyrite and Its Effect on Flotation: Part II. Effect of Grinding on Flotation." International Journal of Mineral Processing, vol. 78, no. 3, 2006, pp. 198–213.

16. Huang, G. Z., and S. Grano. "Electrochemical Interaction of Bornite with Grinding Media and Its Effect on Flotation." Mineral Processing and Extractive Metallurgy, vol. 117, no. 4, 2008, pp. 214–220.

17. Meulendyke, M.J., Moroz, P.J. & Smith, D.M. "Practical aspects of corrosion in the wear of grinding media." Mining, Metallurgy & Exploration 4, 72–77 (1987).

18. Meulendyke, M. J., and J. D. Purdue. "Wear of Grinding Media in the Mineral Processing Industry: An Overview - Mining, Metallurgy & Exploration." SpringerLink, Springer International Publishing, 1 Nov. 1989.

19. ASTM Standard E3-11, 2017, "Standard Guide for Preparation of Metallographic Specimens," ASTM International, DOI: 10.1520/E0003-11R17

20. Andrade, C., and C. Alonso. "Test Methods for on-Site Corrosion Rate Measurement of Steel Reinforcement in Concrete by Means of the Polarization Resistance Method - Materials and Structures." SpringerLink, Kluwer Academic Publishers

21. Krauss, George, and George Krauss. "Chapter 12: Stainless Steels.", "Chapter 14: Cast Irons." *Steels: Heat Treatment and Processing Principles*, ASM International, Materials Park, OH, 1990.

22. Macdonald, D. D. "Passivity–the Key to Our Metals-Based Civilization." Pure and Applied Chemistry, vol. 71, no. 6, 1999, pp. 951–978.

23. ASTM Standard E2594-20, 2020, "Standard Test Method for Analysis of Nickel Alloys by Inductively Coupled Plasma Atomic Emission Spectrometry (Performance-based)," ASTM International, DOI: 10.1520/E2594-20.

24. ASTM Standard E1019-18, 2018, "Standard Test Methods for Determination of Carbon, Sulfur, Nitrogen, and Oxygen in Steel, Iron, Nickel, and Cobalt Alloys by Various Combustion and Inert Gas Fusion Techniques," ASTM International, DOI: 10.1520/E1019-18.

SECTION

3. CONCLUSIONS AND RECOMMENDATIONS

3.1. CONCLUSIONS

The corrosion rates and potentials of various modern grinding media have been measured. Without surprise, HCWI generally exhibits greater E_{corr} and lesser V_{corr} values than HCS. Chloride concentrations of 1 to 4 grams per liter did not affect the corrosion values using the electrochemical methods used in this study. Simulated mill water with lower pH levels caused the corrosion rates of both materials to increase. The presence of dissolved oxygen caused the corrosion rates and potentials to increase compared to deaerated tests. The E_{corr} and V_{corr} values for deaerated tests were scattered and difficult to interpret. Increasing the chromium content of the media generally decreased the corrosion rates and increased the corrosion potentials above 15 wt.% Cr.

Galvanic coupling interactions between HCWI and HCS could be present in most environments examined. The surface area ratio analyses in both papers aim to model corrosion rates for mixed charge ball mill operations. When performing a MBWT in a HCS charge, the HCWI:HCS surface area ratio can be low and affect corrosion rates of both materials. Certain conditions were shown to decrease HCWI's corrosion rate 2 to 93 times when coupled with HCS. Even small additions (10:1 HCWI:HCS) of HCS to a HCWI charge could possibly lower the corrosion rates of the HCWI host material. Galvanic interactions between HCS and HCWI are also greater when the HCWI's

chromium content is increased. Therefore, MBWTs can be affected by galvanic coupling and could cause the overall wear rate to be misrepresented by a change in corrosion rate.

The galvanic coupling models could be used to propose economically attractive charge ratios for operating at optimal grinding media consumption rates. While every milling operation has its own unique minerals and environments, providing models with simple simulated mill water compositions can serve as a baseline for further testing.

3.2. RECOMMENDATIONS

Galvanic interactions between minerals and media as well as dissimilar medias have been studied, but interactions between mill liner and media have not been thoroughly explored. Electrochemical testing of mill liners should be performed to understand the interactions between all materials present in a ball mill.

Further testing should be performed to combine the effects of galvanic coupling on impact and abrasion. Jet-slurry testing [16, 17] combined with a galvanic coupling analysis could lead to interesting results that could help further explain what is happening during a MBWT.

This study focused on the galvanic interactions occurring during MBWTs. Using these surface area ratio analyses could help consumption rates by operating with a mixed charge. An economic justification to use HCS grinding media as a sacrificial anode to protect the HCWI media could impact consumption rates.

BIBLIOGRAPHY

1. Kawatra, S. K., et al. "Chapter 3.8: Grinding Circuit Design." SME Mineral Processing & Extractive Metallurgy Handbook, Society for Mining, Metallurgy & Exploration, Inc., Englewood, CO, 2019.

2. Isaacson, A. E. Effect of Sulfide Minerals on Ferrous Alloy Grinding Media Corrosion. U.S. Dept. of the Interior, Bureau of Mines, 1989

3. Vermeulen, L.A., and D.D. Howat. "Theories of Ball Wear and the Results of a Marked-Ball Test in Ball Milling." Journal of the Southern African Institute of Mining and Metallurgy, vol. 83, no. 8, 1 Aug. 1983.

4. H. Abd-El-Kader, S.M. El-Raghy, Wear-corrosion mechanism of stainless steel in chloride media, Corrosion Science, Volume 26, Issue 8, 1986, Pages 647-653, ISSN 0010-938X.

5. Wang, Jiamei, et al. "Effects of Corrosion Potential, Dissolved Oxygen, and Chloride on the Stress Corrosion Cracking Susceptibility of a 316ng Stainless Steel Weld Joint." CORROSION, vol. 75, no. 8, 2019, pp. 946–959.

6. Tait, W. S. "Effect of Physical Parameters on the Pitting Corrosion of Mild Steel in Low Total Dissolved Solids, Oxygen Bearing Waters: A Nonpassivating Metal/Environment System." Corrosion, vol. 35, no. 7, 1979, pp. 296–300.

7. Adam, K., et al. "Electrochemical Aspects of Grinding Media-Mineral Interaction in Sulfide Ore Grinding." CORROSION, vol. 42, no. 8, 1986, pp. 440–447.

8. Zumelzu, E, et al. "Wear and Corrosion Behaviour of High-Chromium (14–30% CR) Cast Iron Alloys." Journal of Materials Processing Technology, vol. 128, no. 1-3, 2002, pp. 250–255.

9. Lu, Baotong, et al. "Corrosion and Wear Resistance of Chrome White Irons—a Correlation to Their Composition and Microstructure." Metallurgical and Materials Transactions A, vol. 37, no. 10, 2006, pp. 3029–3038.

10. Tang, X.H., et al. "Variations in Microstructure of High Chromium Cast Irons and Resultant Changes in Resistance to Wear, Corrosion and Corrosive Wear." Wear, vol. 267, no. 1-4, 2009, pp. 116–121.

11. Meulendyke, M.J., Moroz, P.J. & Smith, D.M. "Practical aspects of corrosion in the wear of grinding media." Mining, Metallurgy & Exploration 4, 72–77 (1987).

12. Meulendyke, M. J., and J. D. Purdue. "Wear of Grinding Media in the Mineral Processing Industry: An Overview - Mining, Metallurgy & Exploration." SpringerLink, Springer International Publishing, 1 Nov. 1989.

13. Natarajan, K.A., and I. Iwasaki. "Electrochemical Aspects of Grinding Ball-Mineral Interactions in Ore Grinding." Key Engineering Materials, vol. 20-28, 1991, pp. 799–803.

14. Vathsala, and K.A. Natarajan. "Some Electrochemical Aspects of Grinding Media Corrosion and Sphalerite Flotation." International Journal of Mineral Processing, vol. 26, no. 3-4, 1989, pp. 193–203.

15. Huang, Guozhi, et al. "Galvanic Interaction between Grinding Media and Arsenopyrite and Its Effect on Flotation: Part II. Effect of Grinding on Flotation." International Journal of Mineral Processing, vol. 78, no. 3, 2006, pp. 198–213.

16. Huang, G. Z., and S. Grano. "Electrochemical Interaction of Bornite with Grinding Media and Its Effect on Flotation." Mineral Processing and Extractive Metallurgy, vol. 117, no. 4, 2008, pp. 214–220.,

17. Gundewar, C.S., et al. "Studies on Ball Wear in the Grinding of Kudremukh Hematite-Magnetite Ore." Minerals Engineering, vol. 3, no. 1-2, 1990, pp. 207–220.

18. Iwasaki, I., et al. "Nature of Corrosive and Abrasive Wear in Ball Mill Grinding." International Journal of Mineral Processing, vol. 22, no. 1-4, 1988, pp. 345–360.

19. Aldrich, Chris. "Consumption of Steel Grinding Media in Mills – a Review." Minerals Engineering, vol. 49, 2013, pp. 77–91.

20. Norman, T. E., and C. M. Loeb. "Wear Tests on Grinding Balls ." *American Institute of Mining and Metallurgical Engineers*, no. No. 2319, Apr. 1948.

21. West, G. D., and J. D. Purdue. "Marked Ball Wear Testing." 23rd Canadian Mineral Processors Conference, Ottawa, Ontario, Jan. 1991.

22. Sepúlveda, J. E. (2004). Methodologies for the evaluation of grinding media consumption rates at full plant scale. Minerals engineering, 17(11-12), 1269-1279.

23. Tylczak, J. H., Hawk, J. A., & Wilson, R. D. (1999). A comparison of laboratory abrasion and field wear results. Wear, 225, 1059-1069.

24. Blickensderfer, R., & Tylczak, J. H. (1985). Laboratory tests of spalling, breaking, and abrasion of wear-resistant alloys used in mining and mineral processing (Vol. 8968). US Department of the Interior, Bureau of Mines.

25. Tolley, William K., Ivan L. Nichols, and J. L. Huiatt. "Corrosion rates of grinding media in mill water." USBM Report of Investigations 8882 (1984).

26. Gateman, Samantha Michelle, et al. "Using Macro and Micro Electrochemical Methods to Understand the Corrosion Behavior of Stainless Steel Thermal Spray Coatings." Npj Materials Degradation, vol. 3, no. 1, 2019.

27. Massola, Camila Peres, et al. "A Discussion on the Measurement of Grinding Media Wear." Journal of Materials Research and Technology, vol. 5, no. 3, 2016, pp. 282–288.

28. Pitt, C. H., and Y. M. Chang. "Jet Slurry Corrosive Wear of High-Chromium Cast Iron and High-Carbon Steel Grinding Ball Alloys." CORROSION, vol. 42, no. 6, 1986, pp. 312–317.

29. Pitt, C.H., et al. "Laboratory Abrasion and Electrochemical Test Methods as a Means of Determining Mechanism and Rates of Corrosion and Wear in Ball Mills." International Journal of Mineral Processing, vol. 22, no. 1-4, 1988, pp. 361–380.

30. Fontana, Mars G. *Corrosion Engineering*. Tata McGraw-Hill, 1986.

31. Cost of Corrosion Study Unveiled - AMPP. http://impact.nace.org/documents/ccsupp.pdf.

32. Rajendran, Susai, and Gurmeet Singh. *Titanic Corrosion*. Jenny Stanford Publishing, 2020.

33. Mansfeld, Florian. "Tafel Slopes and Corrosion Rates from Polarization Resistance Measurements." Corrosion, vol. 29, no. 10, 1973, pp. 397–402.

34. Andrade, C., and C. Alonso. "Test Methods for on-Site Corrosion Rate Measurement of Steel Reinforcement in Concrete by Means of the Polarization Resistance Method - Materials and Structures." SpringerLink, Kluwer Academic Publishers.

35. Shinagawa, Tatsuya, et al. "Insight on Tafel Slopes from a Microkinetic Analysis of Aqueous Electrocatalysis for Energy Conversion." Scientific Reports, vol. 5, no. 1, 2015.

36. Le Bozec, N., et al. "Influence of Stainless Steel Surface Treatment on the Oxygen Reduction Reaction in Seawater." Corrosion Science, vol. 43, no. 4, 2001, pp. 765–786.

37. Macdonald, D. D. "Passivity–the Key to Our Metals-Based Civilization." Pure and Applied Chemistry, vol. 71, no. 6, 1999, pp. 951–978.

38. Davis, Joseph R., ed. (1994). Stainless Steels. ASM Specialty Handbook. Materials Park, OH: ASM International. ISBN 9780871705037

39. Toma, D., Brandl, W. & Marginean, G. Wear and corrosion behaviour of thermally sprayed cermet coatings. Surf. Coat. Technol. 138, 149–158 (2001)

40. Tang, D.-Z., et al. "Effect of Ph Value on Corrosion of Carbon Steel under an Applied Alternating Current." Materials and Corrosion, vol. 66, no. 12, 2015, pp. 1467–1479.

41. Malik, A.U., et al. "The Influence of Ph and Chloride Concentration on the Corrosion Behaviour of Aisi 316L Steel in Aqueous Solutions." Corrosion Science, vol. 33, no. 11, 1992, pp. 1809–1827.

42. Zhou, Wen. "Effect of a High Concentration of Chloride Ions on the Corrosion Behaviour of X80 Pipeline Steel in 0.5 Mol L-1 nahco3 Solutions." International Journal of Electrochemical Science, 2018, pp. 1283–1292.

43. Lee, Siaw Foon, et al. "Pitting Corrosion Induced on High-Strength High Carbon Steel Wire in High Alkaline Deaerated Chloride Electrolyte." Nanotechnology Reviews, vol. 11, no. 1, 2022, pp. 973–986.

44. Qiu, Jie, et al. "Effect of Chloride on the Pitting Corrosion of Carbon Steel in Alkaline Solutions." Journal of The Electrochemical Society, vol. 169, no. 3, 2022, p. 031501.

45. Parangusan, Hemalatha, et al. "A Review of Passivity Breakdown on Metal Surfaces: Influence of Chloride- and Sulfide-Ion Concentrations, Temperature, and Ph." Emergent Materials, vol. 4, no. 5, 2021, pp. 1187–1203.

46. Jun, Jiheon, et al. "Pitting Corrosion of Very Clean Type 304 Stainless Steel." Corrosion, vol. 70, no. 2, 2013, pp. 146–155.

47. Jankovic, A., et al. "A Comparison of Wear Rates of Ball Mill Grinding Media." Journal of Mining and Metallurgy A: Mining, vol. 52, no. 1, 2016, pp. 1–10.

48. Lin, Bin, et al. "A Study on the Initiation of Pitting Corrosion in Carbon Steel in Chloride-Containing Media Using Scanning Electrochemical Probes." Electrochimica Acta, vol. 55, no. 22, 2010, pp. 6542–6545.

49. Kerber, Susan J., and John Tverberg. "STAINLESS STEEL." Advanced Materials & Processes, vol. 158, no. 5, Nov. 2000, p. 33. Gale Academic OneFile

50. Krauss, George, and George Krauss. "Chapter 12: Stainless Steels.", "Chapter 14: Cast Irons." *Steels: Heat Treatment and Processing Principles*, ASM International, Materials Park, OH, 1990.

51. Xu, Yunze et al. "Experimental Study on Rebar Corrosion Using the Galvanic Sensor Combined with the Electronic Resistance Technique." Sensors (Basel, Switzerland) vol. 16,9 1451. 8 Sep. 2016, doi:10.3390/s16091451

52. Park, Il-Cho, and Seong-Jong Kim. "Determination of Corrosion Protection Current Density Requirement of Zinc Sacrificial Anode for Corrosion Protection of AA5083-H321 in Seawater." Applied Surface Science, vol. 509, 2020, p. 145346.

53. Lavrenko, V. A., et al. "Electrochemical Behavior of ATsKM Sacrificial Anodes in the Course of Long-Term Operation on Seagoing Ships." Materials Science, vol. 40, no. 5, 2004, pp. 687–691.

54. Klopfer, Danny J., and Jeff Schramuk. "A Sacrificial Anode Retrofit Program for Existing Cast-Iron Distribution Water Mains." Journal - American Water Works Association, vol. 97, no. 12, 2005, pp. 50–55.

55. Wahlquist, K. D., and Oliver Osborn. "Magnesium for Cathodic Protection of a Municipal Piping System." Journal - American Water Works Association, vol. 40, no. 5, 1948, pp. 495–503.

56. Greet, Christopher J. "A Protocol for Conducting and Analysing Plant Trials: Testing of High-Chrome Grinding Media for Improved Metallurgy." The Southern African Institute of Mining and Metallurgy, 2012

57. Meier, G.H. "A Review of Advances in High-Temperature Corrosion." *Materials Science and Engineering: A*, vol. 120-121, Mar. 1989, pp. 1–11.

VITA

John Bailey Fletcher earned his bachelor of science in Metallurgical Engineering from the Missouri University of Science and Technology in May 2021. During this time, he had a few internships and participated in undergraduate research with Professor Michael Moats.

He earned his master of science in Metallurgical Engineering from the Missouri University of Science and Technology in July 2022.